A Study of Dynamic Force Measurement Based on the Levitation Mass Method

Tao Jin

Submitted in Partial Fulfillment of the
Requirements for the Degree
of Doctor of Philosophy
in the Graduate School of Gunma University

GUNMA UNIVERSITY

March 2013

ABSTRACT

In this thesis, methods based on the levitation mass method (LMM) for evaluating the frictional characteristics of a linear ball bearing, the electro-mechanical characteristics of a voice coil and a piezo-electric actuator and for removing the velocity limitation of laser Doppler interferometer (LDI) are proposed.

In the LMM, the inertial force of a levitated mass used as the reference force for measuring dynamic force is measured as the product of the mass and acceleration. For evaluating the dynamical friction of linear ball bearing, two corner-cube prisms (CC) are attached to a moving part which is connected to the ball bearing. The acceleration of the gravity center of the moving part is estimated from the accelerations of the two CCs which are measured using a dual axis LDI. The frictional force is measured as the product of the mass of the moving part and the acceleration of the gravity center. For evaluating the voice coil actuator, a moving part levitated using an aerostatic linear bearing is connected to the coil. The dynamic force generated by the coil is measured as the inertial force of the moving part. The velocity of the moving part is measured using a LDI. Other mechanical characteristics such as position, acceleration and force are calculated from the measured velocity. With the electrical characteristics measured using a digital voltmeter, the relationships between electrical and mechanical characteristics are evaluated. For measuring the electro-mechanical characteristics of piezo-electric actuator, a CC considered as an inertial mass is attached to the top of the actuator instead of the moving part. The dynamic force generated by the actuator is measured as the inertial force of CC. Based on this method, the force-displacement behavior of the actuator under dynamic condition is evaluated. The relationship of energy conversion between electrical and mechanical domains is also evaluated based on the observed results.

In the LMM, the velocity of moving part is measured using a LDI whose laser source is a Zeeman-type two-frequency laser. However, the measurable velocity of

LDI is limited by the frequency difference of laser in back and forth motion. In order to get high measurable velocity in back and forth motion, a dual beat-frequencies laser Doppler interferometer (DB-LDI) is developed and applied. In DB-LDI, two laser beams with difference frequency (f_1, f_2) are divided into reference beams and signal beams by a non-polarized beams splitter. They are used to produce two beat signals. When the object moving, the beat frequencies of beat signals are detected as $|f_1^{'} - f_2|$ and $|f_2^{'} - f_1|$, respectively. For back and forth motion, although the velocity of the object calculated from one beat frequency reaches critical velocity, the velocity calculated from the other one is far from critical velocity. The DB-LDI has been applied to realize a high-speed impact testing. During the collision, the velocity of the mass, even higher than the critical velocity, is accurately measured using the DB-LDI.

Contents

List of Figures

List of Tables

Chapter 1

Introduction

Recently, there has been an increasing need for measuring dynamic force in various industrial and research applications such as process monitoring, material testing, motion control and crash testing. However, only static calibration methods are widely available at present, in which the transducers are calibrated with static weights under static conditions. At present, there are no standard methods for calibrating force transducers under dynamic conditions. This leads a problem that the uncertainty is very difficult to determine in measuring a varying or dynamic force by using force transducers. Therefore, the establishment of a dynamic calibration method, with an uncertainty level of a few percent, would be a significant contribution to the field of dynamic force measurement.

Force is one of the most basic mechanical quantities and is defined as the product of mass and acceleration:

$$F = Ma \tag{1.1}$$

where F is the net force acting on the object, M and a are the mass and the acceleration of the center of gravity of the object, respectively. The formula (1.1) implies that the acceleration of the object is directly proportional to the net force acting on the object if the mass of an object is constant. This means that an accurately known acceleration is required to know the net force accurately and to calibrate force trans-

ducers accurately. Due to gravity, g, acceleration is convenient and typically used for generating and measuring constant force. Constant force can be accurately compared using a conventional balance with a knife-edge or a hinge. For measuring and calibrating the varying or dynamic force, an optical method, levitation mass method (LMM), has been proposed by Y.Fujii based on formula (1.1) [1–6, 12, 13].

1.1 Review of dynamic calibration methods

The principle of the LMM is shown in figure 1.1. In the LMM, a mass is levitated by using an linear air bearing. The inertial force $F_{inertial}$ of the levitated mass as a reference force is measured as:

$$F_{inertial} = Ma$$

where M and a are the mass and acceleration of the levitated mass, respectively. The acceleration is accurately measured using an optical interferometer.

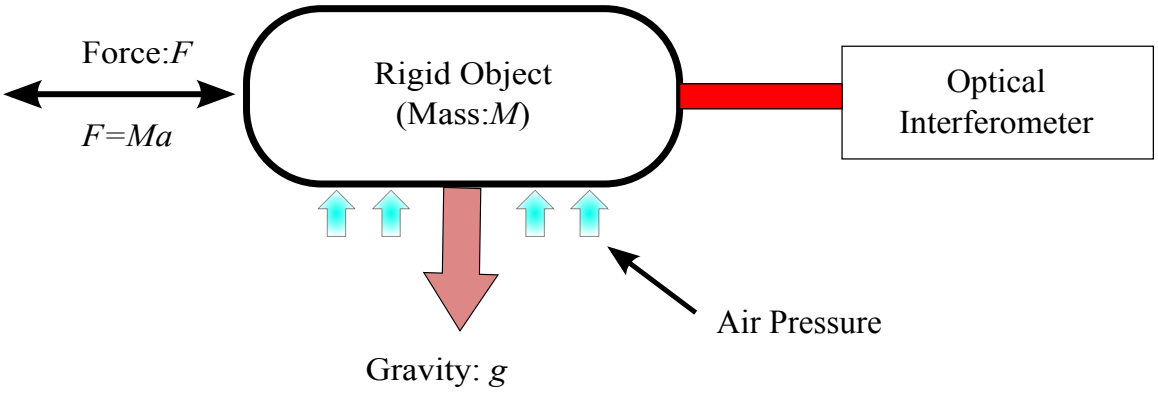

Figure 1.1: Levitation mass method (LMM).

Although the procedures for the dynamic calibration of force transducers are not yet well established, there have been a few attempts to develop dynamic calibration methods for force transducers [1–13]. These attempts can be divided into three categories, namely, methods for calibrating transducers by using impact force, methods

for calibrating transducers by using oscillation force, and methods for calibrating transducers by using step force.

1.1.1 Impact force calibration

A method for calibrating force transducer against impact force is proposed by Y. Fujii [1–6]. Bruns and Kobusch have also developed a similar method for calibrating transducers using impact force [7]. This method was first proposed [2] as an impulse response evaluation method for force transducers; a mass was made to collide with a force transducer and the impulse, i.e., the time integration of the impact force, was measured highly accurately as a change in the momentum of the mass. To obtain linear motion, with a sufficiently small friction acting on the mass, a pneumatic linear bearing [1,3] was used, and the velocity of the mass (i.e., the moving part of the bearing) was measured using an optical interferometer. This method was subsequently improved [4] as a method for determining the instantaneous value of the impact force in the impulse. In this case, the instantaneous value of the impact force was measured as the inertial force acting on the mass, by measuring the instantaneous acceleration of the mass. This method was also improved [5] as a method of determining the response against a steep impulse with a full-width half-maximum (FWHM) width of approximately 1 ms.

1.1.2 Oscillation force calibration

As for the procedures for calibrating transducers against oscillation force, Kumme has proposed and developed a method, in which the inertial force of a mass attached to a force transducer is used [8,9]. In this method, both the mass and the transducer are shaken at a single frequency using a shaker, and the inertial force of the mass is applied to the transducer. The inertial force of part of the transducer itself must be taken into account, to evaluate the characteristics of the transducer under typical conditions in which it is fixed to a stable base. Park et al. used this method for

dynamic investigation of multi-component force-moment sensors [10,11]. Y. Fujii has also proposed a method for calibrating force transducers against an oscillation force, in which the force transducer under test is firmly fixed to a stable base [12].

1.1.3 Step force calibration

As for the procedures for calibrating transducers using step force, Y. Fujii first proposed a method in reference [13]. In this method, the reference force, which is suddenly applied to the force transducer under test, is the combined gravitational and inertial force acting on the object. At the beginning of the evaluation, the object is suspended just above the transducer with the use of a wire; the object is then allowed to fall onto the transducer by cutting the wire. To realize perpendicular motion with insignificant friction, a pneumatic linear bearing is used. The inertial force of the object is measured highly accurately by measuring the velocity of the mass using an optical interferometer. In addition, the step force response of force transducers has recently become a topic of much interest. For example, there is research dealing with the dynamic characteristics of force transducers under step load [14]. In this method, the real force is approximately estimated from the output signal without the knowledge of the reference force. Strictly speaking, there are no other dynamic calibration methods using a step force, in which a known step force is used as the reference, except the method proposed by Y. Fujii.

In summary, the present status of dynamic force measurement is as follows: methods have been proposed and developed for the dynamic force calibration of force transducers against some typical types of dynamic forces such as impact force, oscillation force and step force. However, it has not been established how to apply the results of such dynamic calibration to the actual wave profile of the varying force. This difficulty mainly comes from the fact that the validity of applying the frequency response obtained from the oscillation force calibration to other types of force such as impact force and step force has not been proved. On the other hand, the fact that

there are no standard methods for evaluating the dynamic characteristics of force transducers results in two major problems concerning material testing.

1. One is that it is difficult to evaluate the uncertainty in the measured value of the varying force.

2. The other is that it is difficult to evaluate the uncertainty in the time at which the varying force is measured.

In this situation, the methods for evaluating the mechanical properties of materials such as viscoelasticity and hysteresis in dynamic conditions have been proposed based on LMM. The advantages of these methods are listed as following:

- Due to the high precision of today's mass standards with relative uncertainties of less than 10^{-6}, the mass that contributes to the measurement uncertainty of measurement can be neglected.

- The friction force of the air bearing applied on mass is small enough [1,3]. The uncertainly of measurement can be neglected.

- The acceleration is accurately measured by using a laser interferometer. It's an absolute measuring method, which is used in national acceleration standards with the best accuracy [15].

- All the necessary mechanical quantities such as velocity, displacement, acceleration and force are calculated from the Doppler frequency shift only.

Table 1.1 shows the advantages of the LMM in dynamic force measurement. The main advantage of the LMM that the uncertainly of the dynamic force measurement can be estimated. This is very important, for example, when dynamic testing materials, the uncertainly of dynamic force can not be estimated by using force transducers. While, by using LMM, this problem can be resolved. The accuracy of the LMM based on the accuracy of Doppler frequency estimation.

Table 1.1: Comparison of dynamic force measurement methods.

Methods	Application	Size	Cost	Uncertainty
Force transducer	Easy	Small (only transducer)	Cheap ($500∼)	cannot be estimated
LMM	Difficult (sometimes need some ideas)	Large (Interferometer and air bearing)	Expensive ($10,000∼)	based on the uncertainty of mass and acceleration measurement

1.2 Aims

Because of the high precision, LMM is modified and applied in transducer calibration, materials testing and mass measuring in dynamic condition. In order to improve the performance of LMM and increase the application of LMM, this thesis focuses on the following listed aims:

1. To evaluate the electro-mechanical characteristics of materials under test and the friction of linear ball bearings under dynamic condition.

2. To develop a new material tester, in which the measurable collision velocity is not limited by the laser Doppler interferometer.

3. To remove the intensity noise of beat beams.

1.3 Structure of the thesis

The LMM has been applied in dynamic calibration, material testing and mass measurement, however, how to extend the application and improve the precision of LMM is still urgently required. Based on these issues, some recent works for LMM are reported in this thesis. The thesis is organized as follows:

Chapter 1 describes the principle of LMM and reviews the methods based on LMM for calibrating force transducer and testing materials.

Chapter 2 reports the methods for improving LMM and the applications based on LMM: (1). In section 2.1, the dynamic fraction of a linear ball bearing is evaluated. In addition, the pitching angle of the linear ball bearing is also precisely measured. (2). In section 2.2, we applied LMM to estimate the electro-mechanical characteristics of a voice coil actuator. By using a voltmeter, the relationships between electrical and mechanical characteristics are evaluated. The experimental results are a great help to understand and control the voice coil actuator during dynamic condition. (3). In section 2.3, we applied LMM to estimate the electro-mechanical characteristics of piezo-electric actuators. In this section the structure of LMM is modified comparing with the experimental setup for evaluating the voice coil. The moving part of LMM is replaced by a corner-cube prism which is attached on the top of a actuator directly. (4). In section 2.4, a dual beat-frequencies laser Doppler interferometer (DB-LDI) is proposed and used in order to remove the limitation of measurable velocity of laser Doppler interferometer. In this interferometer, the two frequencies, f_1 and f_2, emitted by a Zeeman-type two-frequency laser are introduced into the signal beams. They are changed to $f_1^{'}$ and $f_2^{'}$ by Doppler frequency shift which is proportional to the velocity of the object. The use of the two beat signals of $|f_1^{'} - f_2|$ and $|f_1 - f_2^{'}|$ appearing at two photodetectors enables to measure the velocity over the limitation $v_c = \lambda(f_1 - f_2)/2$ or under $-v_c = -\lambda(f_1 - f_2)/2$. The experimental results showed that the limitation of measurable velocity is removed. The impulse response of material with high impact velocity is evaluated by using DB-LDI.

Chapter 3 summarizes the results of the present work and states the future work for improving the performance of LMM.

Chapter 2

Applications of LMM

2.1 Method for evaluating dynamic friction of linear ball bearings

2.1.1 Introduction

The friction of the bearing is of great interest in the field of precision engineering [39–42]. However, techniques for measuring the friction of linear bearings have not been sufficiently investigated. Conventional techniques such as the technique using a force transducer [39] and that using the gravitational force acting on a weight [40–42] do not provide sufficient precision for some applications. Considering the important role of linear bearings, it is essential to develop techniques for evaluating their frictional characteristics with high accuracy.

The LMM has been applied to investigate the frictional characteristics of pneumatic linear bearings [43, 44]. It was also used for investigating the frictional characteristics of linear ball bearings, whose motion is almost linear with negligible pitching vibration [45]. In such methods, no force transducers are used and the force is directly measured based on the definition of force, i.e., the product of mass and acceleration. However, it is still difficult to evaluate the dynamical friction acting on a usual linear

ball bearing, whose motion is not perfectly linear due to some play, which is slack or gap between the moving part and the guide way. The play causes the translational and rotational vibrations of the moving part. The reasons for this difficulty are as follows. (1). The acceleration is measured at the measurement point, i.e., at the optical center of the corner–cube prism. (2). The measurement point and center of gravity of the moving part are separated. (3). The vibration of the moving part due to the slack or play results in a change in the difference between the acceleration of the measurement point and that of the center of gravity of the moving part.

In this section, a novel method for overcoming the above difficulties due to the pitching vibration of the moving part of the bearing is proposed. In the proposed method, the accelerations of two different points on the moving part are measured using a dual-axis optical interferometer. The relative positions between the two measurement points and the center of gravity are evaluated beforehand using the balancing method. The acceleration of the center of gravity is calculated from the accelerations of two measurement points.

2.1.2 Experimental setup

Figure 2.1 shows the experimental setup used for evaluating the frictional characteristics of a linear ball bearing with some play in the internal mechanism. Figure 2.2 shows a photograph depicting the region around the test section. Two corner–cube prisms CC1 and CC2 are attached to the moving part of the bearing. The coordinate system fixed in space (x, y, z) is set as shown in figure 2.1. The coordinate system fixed to the moving part (ξ, η, ζ) is set as shown in figure 2.2. The relative positions of the optical centers of CC1 and CC2 are $P_{cc1} = (\xi_{cc1}, \eta_{cc1}, \zeta_{cc1}) = (75.2\text{ mm}, 0.0\text{ mm}, 12.0\text{ mm})$ and $P_{cc2} = (\xi_{cc2}, \eta_{cc2}, \zeta_{cc2}) = (74.7\text{ mm}, 0.0\text{ mm}, 37.7\text{ mm})$, respectively. The measurement points are P_{CC1} and P_{CC2}. The height difference L between the optical centers of CC1 and CC2 is approximately $L = |\zeta_{cc2} - \zeta_{cc1}| = 25.7$ mm.

If the motion of the moving part is perfectly parallel translation, then the accel-

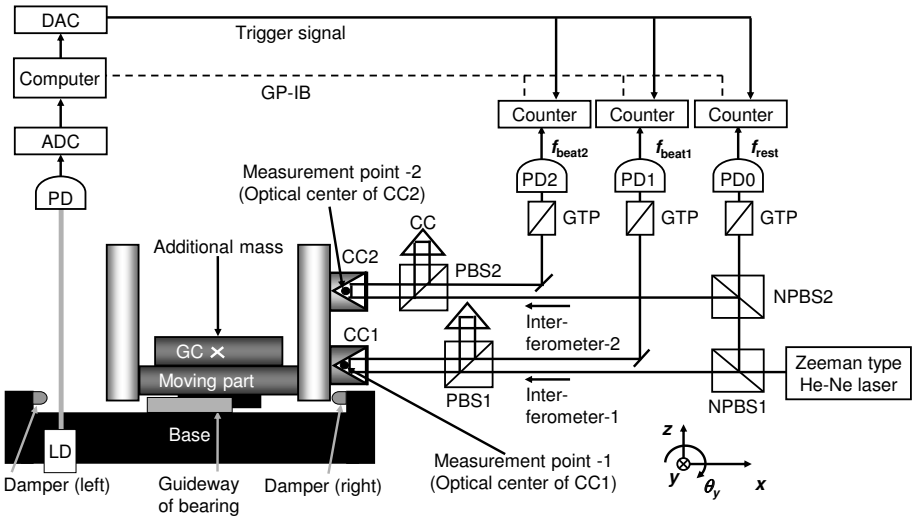

Figure 2.1: Experimental setup for evaluating dynamical friction of linear ball bearings.

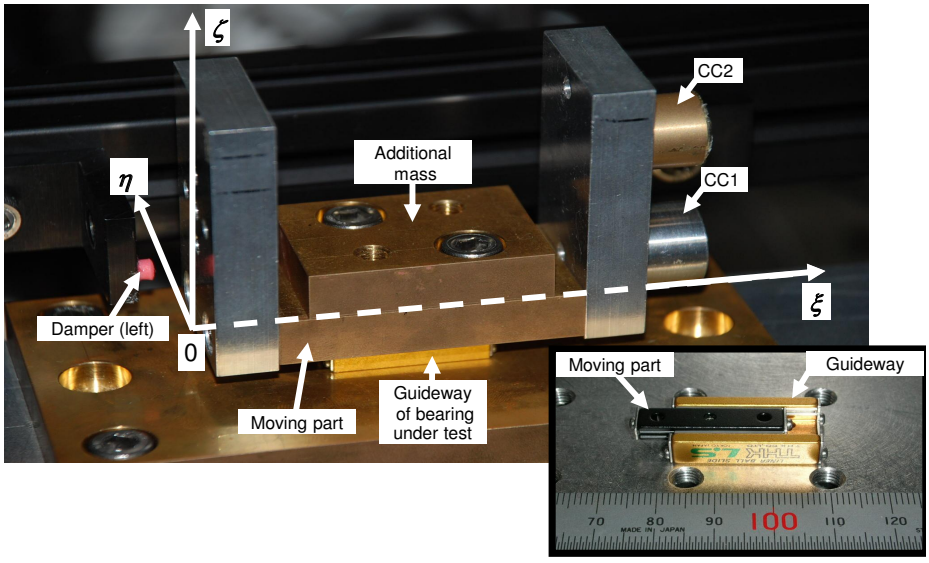

Figure 2.2: Photographs of the bearing under test, on which the coordinate system is shown.

erations of P_{CC1} and P_{CC2} are equal to the acceleration of the center of gravity (GC) of the moving part, P_{GC}. However, if the motion is not parallel translation, then its rotational motion results in the difference of the accelerations of P_{CC1}, P_{CC2} and P_{GC}.

In the proposed method, the acceleration of the center of gravity and the total force acting on the moving part are estimated as follows:

(1). First, P_{GC} is estimated by the balancing method [46] as the following steps. Here, the relative position of the center of gravity (GC) of the moving part, P_{GC}, is thought to be in the $\xi\zeta$ plane since the moving part is symmetrical with respect to the $\xi\zeta$ plane. P_{CC1} and P_{CC2} are also in the plane. Therefore, the differences between the accelerations of P_{CC1}, P_{CC2} and P_{GC} are mainly caused by the rotational motion along y-axis, i.e., the pitching motion.

i) The moving part is separated from the other parts and it is hung using a fine thread at three different points. When the moving part is suspended by a thread from a point, it is in equilibrium under the action of the tension in the thread and the resultant of the gravitational forces of the moving part. When the moving part is suspended from another point, it is again in equilibrium.

ii) Side-view pictures are taken from the η-axis direction, and the straight lines are marked over the thread on these pictures. These lines indicate the lines of action of the resultant of the gravitational forces. These lines would be concurrent at P_{GC}.

iii) From the three pictures, P_{GC} is estimated by means of the least squares method.

P_{GC} is estimated to be $(\xi_{GC}, \eta_{GC}, \zeta_{GC}) = (36.9 \text{ mm}, 0.0 \text{ mm}, 15.8 \text{ mm})$ when one additional mass is attached to the moving part. The height of CC1 is closer to that of the GC as compared to the height of CC2.

(2) Second, the acceleration at P_{GC} in the direction of motion, i.e., direction of x-axis, is estimated using the accelerations at the two measurement points, i.e., the optical centers of CC1 and CC2:

$$a_{GC} = ((\zeta_{CC2} - \zeta_{GC})a_1 + (\zeta_{GC} - \zeta_{CC1})a_2)/(\zeta_{CC2} - \zeta_{CC1}) \tag{2.1}$$

where a_1 and a_2 are the accelerations along x-axis at the optical centers of CC1 and CC2, respectively. Then, the total force acting on the moving part, F, is calculated as the product of the mass of the moving part, M, and the acceleration at the GC,

a_{GC}, as:

$$F = Ma_{GC} \tag{2.2}$$

If only one CC is used and the height difference between the CC and GC is not zero, the acceleration at the CC along the x-axis would be sensitive to the rotation along the y-axis, i.e., the pitching motion, because the pitching motion easily causes the displacement of the CC along the x-axis as the sine error. This causes the measurement error in the acceleration at the GC. Thus, if only one CC is used, the heights of the optical center of the prism and the optical setup should be carefully adjusted to be the same as the height of the GC. In the proposed method, on the other hand, the effect of pitching motion can be corrected by equation (2.1).

As for the effects along the other axes, their effects on the measurement error are thought to be negligible. More specifically, the acceleration along the x-axis is not affected by the rotation along the x-axis, i.e., the rolling motion, at all. It is weekly sensitive to the rotation along the z-axis, i.e., the yawing motion, since that is the cosine error.

A Zeeman-type two-frequency He-Ne laser is used as the light source of the dual-axis optical interferometer. The interferometer has three photodetectors: PD0, PD1 and PD2. The frequency difference between the two orthogonal polarization states emitted from the laser, f_{rest}, is monitored using a Glan-Thompson prism (GTP) and the first photodetector (PD0).

The velocity of CC1, v_1, is measured as the Doppler shift frequency $f_{Doppler1}$, which can be expressed as follows:

$$v_1 = \lambda f_{Doppler1}/2 \tag{2.3}$$

$$f_{Doppler1} = -(f_{beat1} - f_{rest}) \tag{2.4}$$

where λ_{air} is the wavelength of the signal beam under the experimental conditions and f_{beat1} is the beat frequency, which is the frequency difference between the signal beam and the reference beam, that appears at PD1. In the same way, the velocity of

CC2, v_2, is measured as the frequency Doppler shift $f_{Doppler2}$.

The frequency f_{rest} appearing at PD0 is measured using an electric frequency counter (model: R5363; manufactured by Advantest Corp., Japan). It continuously measures and records the rest frequency f_{rest} 2000 times at a sampling interval of T = $4000/f_{rest}$ and stores the values in its memory. This counter continuously measures the interval time every 4000 periods without dead time. The sampling period of the counter is approximately 1.4 ms at a frequency of 2.8 MHz. Two other counters of the same model measure the frequencies f_{beat1} and f_{beat2} appearing at PD1 and PD2, respectively. The counters measure the frequencies without dead time, and T can be exactly calculated using the measured frequency f and the expression T = $4000/f$. The position x is calculated by integrating the velocity v. The acceleration a is calculated by differentiating the velocity v.

The measurements using the three electric counters (R5363) are triggered by means of a sharp trigger signal generated using a digital-to-analog converter (DAC). This signal is initiated by means of a light switch, which is a combination of a laser diode and a photo-diode.

In the experiment, only one additional mass is attached to the moving part. The total mass of the moving part with the additional mass M is 0.311 kg.

2.1.3 Results

Figure 2.3 shows the change in velocity at CC1, v_1, and the velocity at CC2, v_2. During the measurement of approximately 3 seconds, the moving part performs reciprocating motion.

Figure 2.4 shows the change in position at CC1, x_1, the position at CC2, x_2, and the pitching angle of the moving part, θ_y. The positions x_1 and x_2 are calculated by integrating the velocities v_1 and v_2, respectively. The pitching angle θ_y is calculated

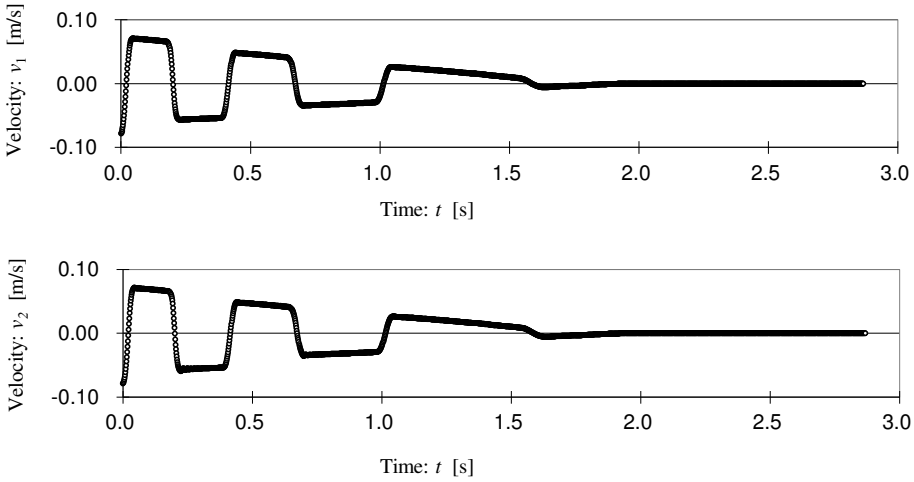

Figure 2.3: Change in velocities at CC1 and CC2.

using the following expression:

$$\theta_y \approx \delta x / L \tag{2.5}$$

$$\delta x = x_{CC2} - x_{CC1} \tag{2.6}$$

where L is the height difference between the optical centers of CC1 and CC2 ($L = |\zeta_{CC2} - \zeta_{CC1}|$). The pitching angle θ_y is the rotation angle around y-axis, and it changes significantly when the moving part collides with the side dampers. It appears that the slack or play of the bearing around the right side is larger than that around the left side.

Figure 2.5 shows the change in acceleration, a_1, at CC1, the acceleration, a_2, at CC2, and the acceleration, a_{GC}, at the GC. The accelerations a_1 and a_2 are calculated by differentiating the velocities v_1 and v_2, respectively. The parameter a_{GC}, i.e. the acceleration at P_{GC} in the direction of motion, is calculated from a_1 and a_2 using equation (2.1). In each figure, the 3 runs of the rightward motion and the 2 runs of the leftward motion are drawn. The acceleration of CC2, whose height differs considerably from that of the GC as compared to the height of CC1, varies considerably. On the other hand, the plotted lines of a_{GC} in different runs of the moving part coincide well

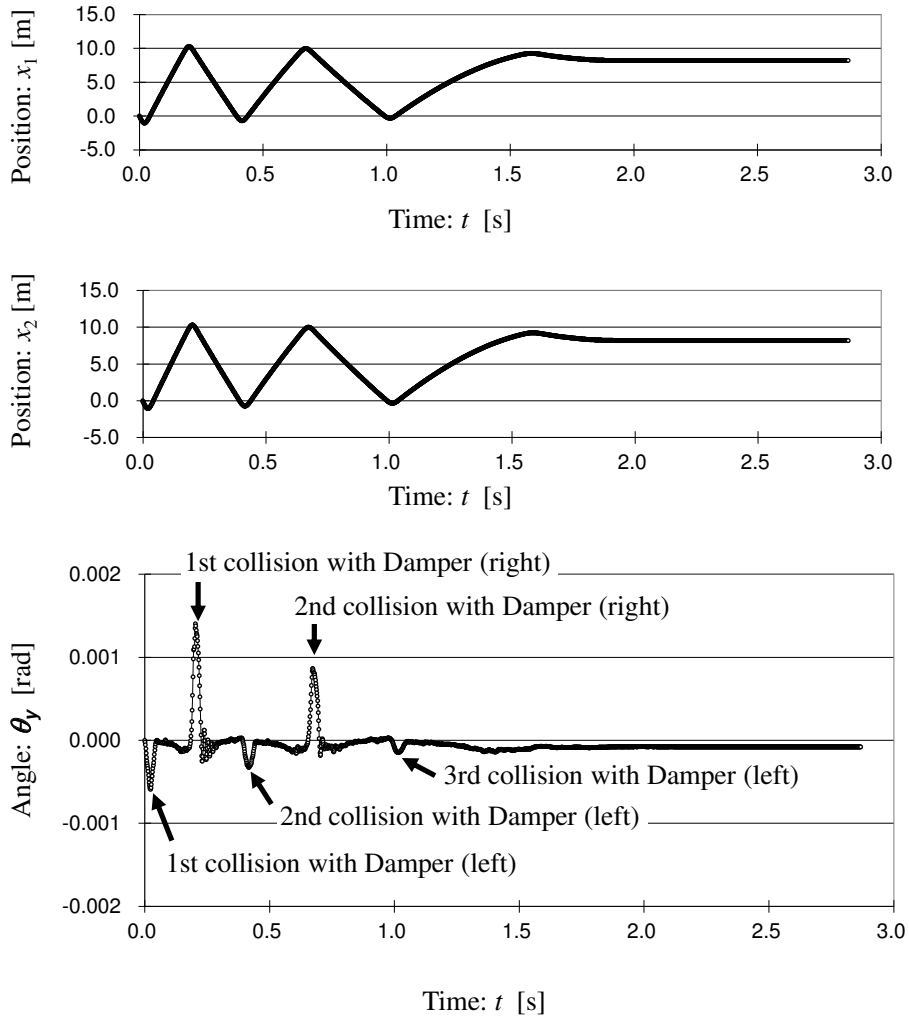

Figure 2.4: Change in positions at CC1 and CC2 and in pitching angle.

with each other.

Figure 2.6 shows the change in the total force F acting on the moving part and the pitching angle of the moving part θ_y against its position. The total force acting on the moving part F is calculated as the product of the mass of the moving part M and the acceleration a_{GC} at the GC. In the figure of F, lines of different passes coincide well with each other. Around the regions indicated as **A** and **B** in the figure, the total force acting on the moving part has a unique feature. These indicate both the high reproducibility of the frictional force acting inside the bearing and the high

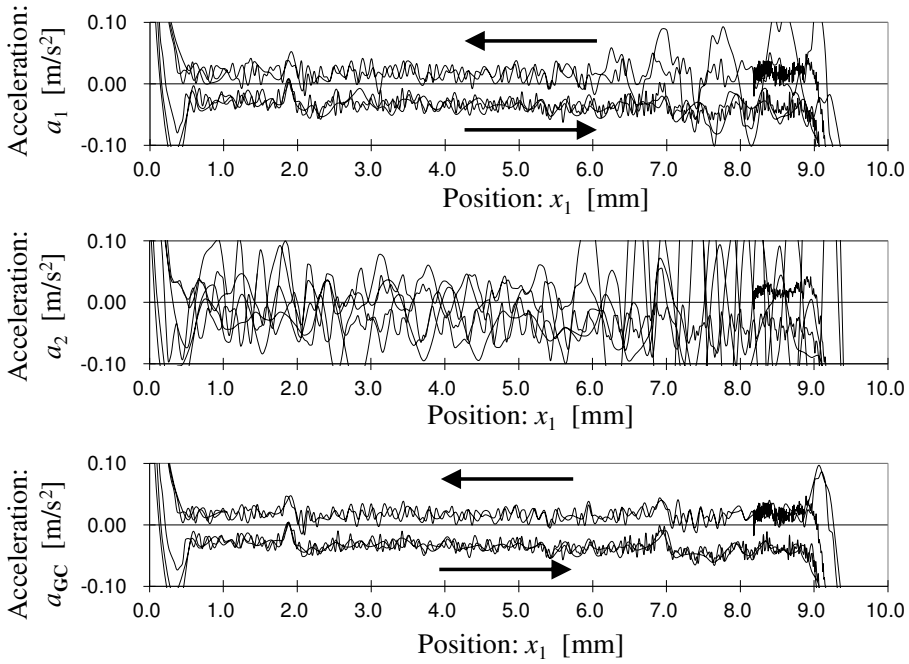

Figure 2.5: Change in acceleration at CC1, CC2 and GC

accuracy of the measurement.

2.1.4 Uncertainty Evaluation

The uncertainty components in determining the instantaneous value of the acceleration at the center of gravity of the moving part a_{GC} are as follows:

(a) Measurement of the accelerations a_1 and a_2. The dominant uncertainty source in the accelerations a_1 and a_2 is the uncertainty in the frequency measurement using the electric frequency counter R5363 of approximately 3 Hz, since the other uncertainty sources, such as the laser alignment, refractive index of air and the wavelength of the laser, are negligible. This corresponds to the uncertainty of the accelerations a_1 and a_2 of approximately 2×10^{-3} m/s^2. This results in the standard uncertainty of a_{GC} due to the uncertainty of the accelerations a_1 and a_2 of approximately 3×10^{-3} m/s^2.

(b) Estimation of P_{GC} The uncertainty in estimating the position of the center

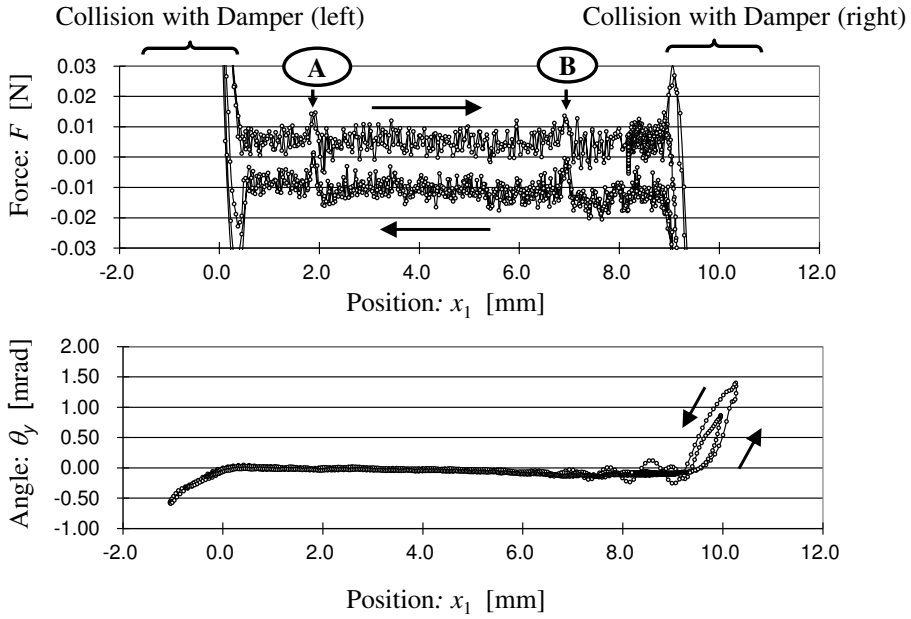

Figure 2.6: Change in total force acting on the moving part and pitching angle of the moving part against position.

of gravity of the moving part P_{GC} is estimated to be approximately 0.1 mm. This corresponds to the standard uncertainty of a_{GC} due to the uncertainty of P_{GC} of approximately 0.4×10^{-3} m/s^2.

Therefore, the standard uncertainty in estimating a_{GC} is estimated to be approximately 3×10^{-3} m/s^2. This corresponds to the standard uncertainty in estimating the total force acting on the moving part of approximately 0.9×10^{-3} N.

2.1.5 Discussion

The plotted lines in different runs of the moving part coincide well each other. The coincidence suggests that the frictional force is measured with high reproducibility even if the velocity of the moving part is changed. Thus, using the proposed method, the frictional characteristics of linear bearings with some play in their mechanism can be accurately evaluated. Conventional linear ball bearings have some play, and

therefore the proposed method will contribute significantly to research on linear ball bearings and the linear ball bearing industry. The evaluation of uncertainty of the method has not been completely done. However, the authors estimate that the relative standard uncertainty in measuring the frictional force is approximately 5 % in the described experiment.

Using the proposed method, the relationships between the time, velocity, acceleration, inertial force, position and pitching angle are accurately measured. Their small changes in the short period can be observed. This will help in understanding the phenomenon and mechanism of frictional force acting inside the linear ball bearing. In the proposed method, only the time-varying frequency is measured during the sliding experiment. The velocity, acceleration, inertial force and position are all calculated from the measured time-varying beat frequency. This induces the synchronization between the calculated physical quantities and the simplicity of the measurement system.

The effect of pitching motion correction with the proposed method on the improvement in the measurement accuracy is significant, as shown in figure 2.5. This fact also indicates that if only one cube-corner prism can be attached to the moving part of the bearing, then the height of the optical center of the prism should be carefully adjusted to be the same as the height of its GC. This adjustment is severe and troublesome especially when the measurement is done for various additional masses. Moreover, the pitching angle cannot be monitored if only one cube-corner prism is used. On the other hand, in the proposed method, the adjustment is not severe and no changes of the height of the optical center of each prism and the optical setup are required even when the additional mass is changed.

In the proposed method, the total mass of the moving part and the relative positions between the two measurement points and the center of gravity should be measured beforehand. Once they are measured under a certain condition of attached masses, then they can be calculated using the mass and the center of gravity of the

additional attached mass. If the shape and the density distribution of the moving part is enough known precisely, then the relative positions between the two measurement points and the center of gravity can be numerically calculated. In this case, no measurement of the center of gravity is necessary.

In the LMM, the measurement of frequency is essential. To improve the sampling interval and the resolution of frequency measurement, the introduction of the novel method [47, 48] using a digitizer instead of an electric counter will be effective.

2.1.6 Conclusions

A novel method for evaluating the frictional characteristics of linear bearings with some play in its mechanism was developed by modifying the levitation mass method (LMM). In the measurement, the moving part of a linear ball bearing was made to move freely, and the force acting on the moving part was measured as the inertial force given by the product of its mass and the acceleration of its center of gravity. To evaluate the acceleration of gravity center of moving part, the acceleration of two different points on it were measured using a dual-axis optical interferometer. The measured results indicated the high reproducibility of the frictional force acting inside the bearing and the high accuracy of the measurement. The precision measurements of the frictional characteristics of the linear ball bearings, which are widely used in many applications of mechanotronics and robotics, will help in understanding the mechanics of friction and in developing an improved method for the position control of linear actuators with linear bearings. The proposed method will contribute significantly to research on linear ball bearings and the linear ball bearing industry.

2.1.7 Future work

In section 2.1, we applied the LMM to estimate the dynamic fractional force of linear ball bearing. As shown in our experiment, the key point in this experiment is how to estimate the gravity center of the moving part. Therefore, in the future work, a more

accuracy method is possible needed to estimate the gravity center. A possible choose is using center-of-gravity attitude model. By using this method, the Euler angle (roll, pitch and yaw angles) can be estimated.

2.2 Method for evaluating the electro-mechanical characteristics of a voice coil actuator

2.2.1 Introduction

High-precision control of linear actuators is required in various industrial and research applications. For realizing the high-precision control, high-precision measurements and models are required. In conventional tester, the force generated by the actuator is measured using a force transducer, and the position of the actuator is measured using a position transducer [49–52]. However, the force transducers are typically calibrated by standard static methods using static weights under static conditions [5]. Therefore, it is difficult to evaluate the uncertainty in the measured varying force and the uncertainty in the moment at which the varying force is measured.

To resolve this problem, LMM is modified and applied to evaluate the electro-mechanical characters of a voice coil actuator when it is driven. In order to measure the dynamic force generated by the actuator, a moving part as inertial mass is connect to the actuator. When the actuator was driven, the inertial force of the moving part, which is measured as the product of mass and acceleration, is considered as the force generated by the actuator. The inertial force is measured using a laser Doppler interferometer. The beat signals are stored into computer by using a low cost digitizer. The frequencies of beat signals are measured using the zero-crossing averaging method. In section 2.2.2, the experimental setup for evaluating the electro-mechanical characteristics of a voice coil actuator is described. The performance of the proposed method is demonstrated.

2.2.2 Experimental setup

Figure 2.7 shows a schematic diagram of the experimental setup for evaluating the electrical and mechanical characteristics of a voice coil actuator. The voice coil ac-

tuator (model: VCM26-02R; manufactured by Showa Electric Wire and Cable Co., Ltd., Japan) is connected to the moving part of an aerostatic linear bearing (model: Air-Slide TAAG10A-02; manufactured by NTN Co., Ltd., Japan). A corner–cube (CC) prism (for the interferometer) and some metal blocks (used for connecting the mass with the actuator) are attached to the moving part; the total mass M is approximately 4.118 kg.

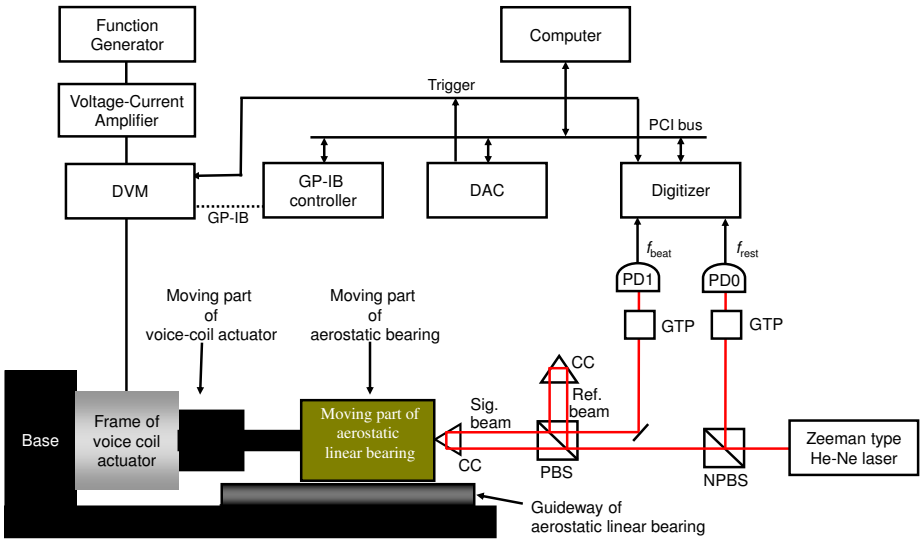

Figure 2.7: Experimental setup for evaluating the electro-mechanical characteristics of voice coil.

A Zeeman-type two-frequency He-Ne laser is used as the light source of the optical interferometer. The interferometer has two photodetectors: PD0 and PD1. The frequency difference f_{rest} between the two orthogonal polarization states emitted from the laser is monitored using a Glan-Thompson prism (GTP) and the first photodetector PD0.

The total force F acting on the moving part of the aerostatic linear bearing is calculated as the product of its mass M and its acceleration a:

$$F = Ma \tag{2.7}$$

The acceleration is calculated from the velocity v of the levitated mass which is

calculated from the Doppler shift frequency $f_{Doppler}$:

$$\begin{aligned} v &= \lambda_{air} f_{Doppler}/2 \\ &= -\lambda(f_{beat} - f_{rest}/2) \end{aligned} \tag{2.8}$$

where λ_{air} is the wavelength of the signal beam under the experimental conditions; f_{beat} is the beat frequency, which is the frequency difference between the signal beam and the reference beam and appears as the beat frequency at PD1; and f_{rest} is the rest frequency, which is the value of f_{beat} when the moving part is at a standstill. The direction of the coordinate system for the velocity, acceleration, and force acting on the moving part is toward the right, as shown in figure 2.7. The position x and the acceleration a of the mass and the force F acting on the mass are numerically calculated from the velocity v.

The frequency is calculated from the waveform recorded using a low-cost digitizer (model: 5102; manufactured by National Instruments Corp., USA) based on the zero-crossing averaging method (ZAM) [58]. The digitizer records the signals from both PD0 and PD1 with 5 M samples for each channel, a sampling rate of 20 MS/s, and 8-bit resolution. The measurement duration of the digitizer is 0.25 s.

As shown in figure 2.8, the frequency f_j is determined from P_j, which is the duration of N periods: $f_j = N/P_j$, where $j \geq 0$. The starting time T_j and the ending time T_{j+1} of the duration P_j are calculated as the average time of $(2n+1)$ adjacent zero crossings, where n is a nonnegative integer and represents the half width of the averaging interval. The time of the zero crossings, $t_i (i = 0, 1, 2, \cdots)$, at which the waveform crosses zero from the negative value to the positive value is determined by linear interpolation using the two adjacent data points. Finally, $P_j (j = 1, 2, 3 \cdots)$ is

calculated as $P_j = T_{j+1} - T_j$, and the frequency is given by $f_j = N/P_j$, i.e.

$$T_j = \frac{1}{2n+1} \sum_{i=jN}^{jN+2n} t_i \tag{2.9}$$

$$P_j = T_{j+1} - T_j \tag{2.10}$$

$$f_j = N/P_j \tag{2.11}$$

In this study, $N = 400$ and $n = 190$. The measurement period is approximately 0.14 ms when the moving part is at a standstill.

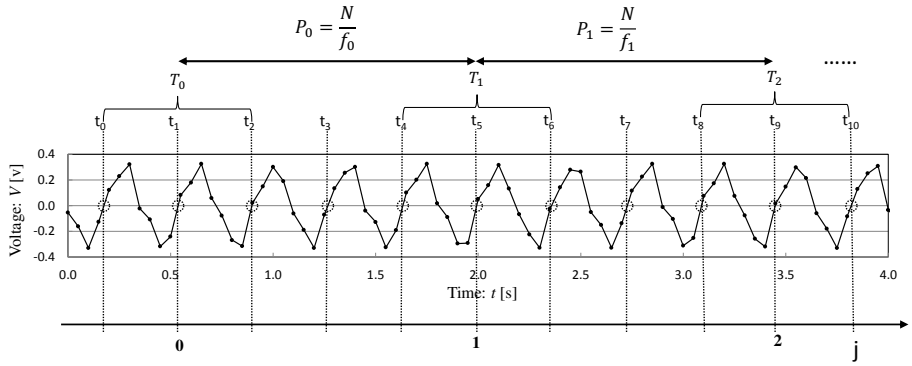

Figure 2.8: Algorithm of zero-crossing averaging method (in the case, n=2, N=4).

The aerostatic linear bearing is attached to an adjustable tilting stage. The maximum weight of the moving part is approximately 30 kg, the thickness of the air film is approximately 8 μm, the stiffness of the air film is more than 70 N/μm, and the straightness of the guideway is better than 0.3 μm/100 mm. The frictional characteristics were determined in detail by means of the developed method [55].

The voice coil actuator is driven by a voltage-current amplifier. A function generator is used to supply a square wave of 35 Hz to the amplifier. The voltage and the current of the actuator are measured using a digital voltmeter (model: VP5481L; manufactured by Panasonic Corp., Japan). The time axis of the measured electrical quantities, namely, current and voltage, is adjusted to that of the mechanical quantities using linear interpolation.

The measurements performed using the digitizer and digital voltmeter are triggered by means of a sharp trigger signal generated by a digital-to-analog converter (DAC). In the experiment, only one oscillation test was conducted and only one set of measurements was obtained.

2.2.3 Results and Discussion

Figure 2.9 shows the mechanical quantities measured during the experiment. First, the frequency is calculated from the digitized output signal of the optical interferometer and then the velocity, position, acceleration, force, and mechanical power are calculated from the frequency. In figure 2.9, approximately 8 periods of the reciprocating motion are observed.

Figure 2.10 shows the electrical quantities measured during the experiment. Although the function generator supplies a square wave of 35 Hz to the voltage-current amplifier, the current exhibits a dull waveform, while the voltage exhibits an overshoot waveform.

Figure 2.11 shows the change in force against current and voltage. It is reasonable and the same as the theoretical estimate that the force F is almost proportional to the current I. The regression line is $F = -2.3I - 0.14$. Fine structures are observed in the curves and they coincide well during the 8 periods of the reciprocating motion. This indicates an accurate performance of the experimental setup and a high reproducibility of the measurements. As shown in figures 2.10 and 2.11, there is noise appeared at the times when the velocity arrived peak value. It's may be that some inertial force of the coil exited at those times.

Figure 2.12 shows the change in force, velocity, and voltage against position. The reproducibility of these results is very high during the 8 periods of the reciprocating motion.

Figure 2.13 shows the relationship between electric power and mechanical power. The energy efficiency of the motor is very poor. The reproducibility of these results

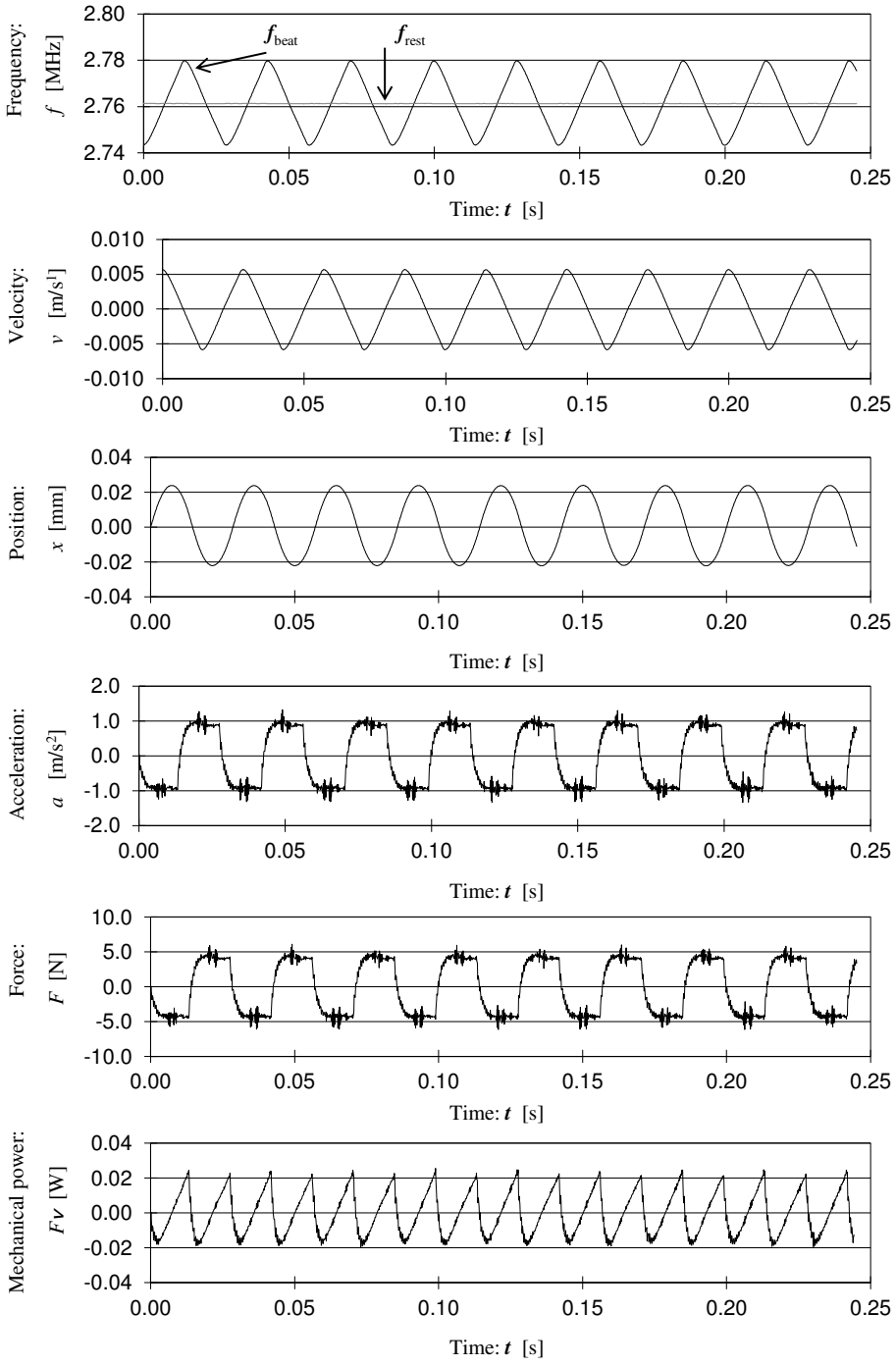

Figure 2.9: Mechanical quantities of the voice coil actuator measured during the experiment.

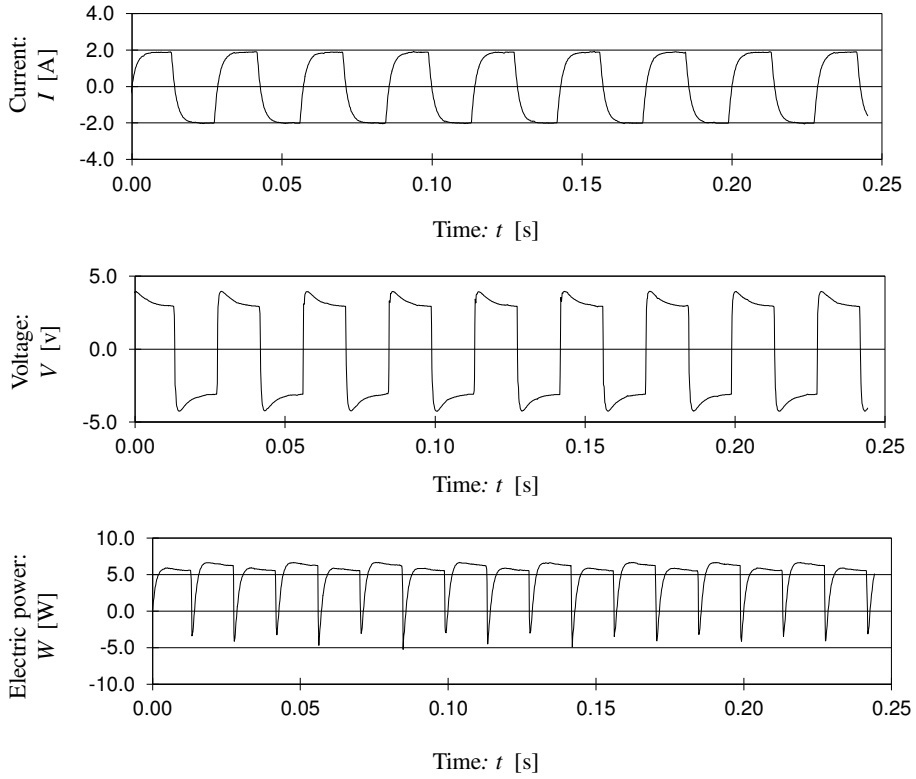

Figure 2.10: Electrical quantities measured during the experiment.

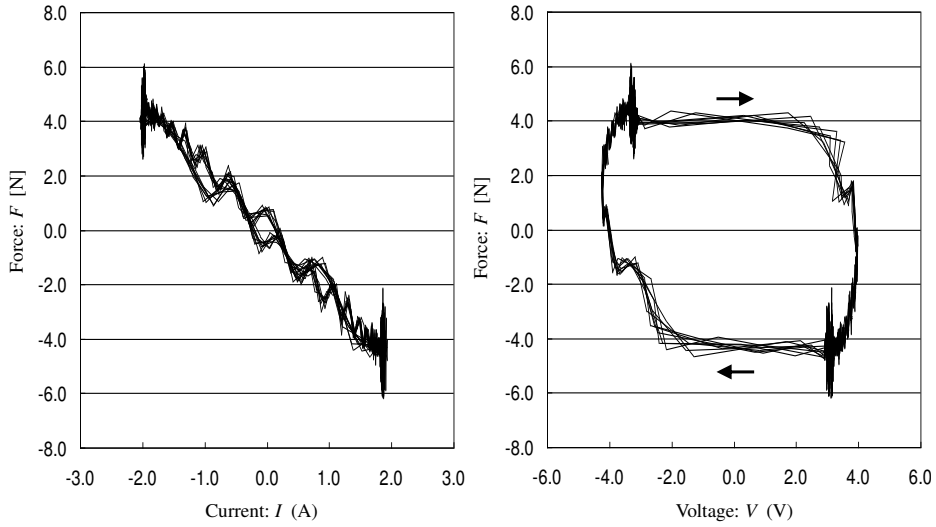

Figure 2.11: Change in force against current and voltage.

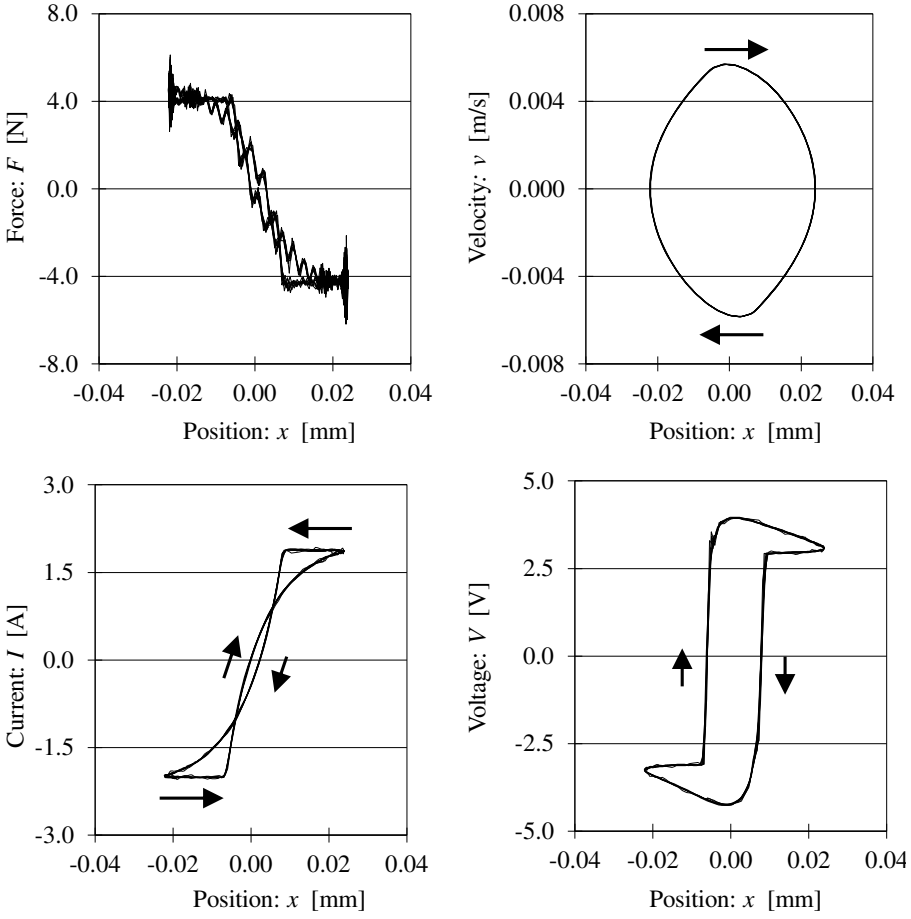

Figure 2.12: Change in force, velocity, current and voltage against position.

is very high during the 8 periods of the reciprocating motion.

The precise measurement data of a voice coil actuator under dynamic conditions will be useful for understanding the phenomenon and the mechanism of its motion. The high-precision measurements of the voice coil actuator realized by the proposed method will contribute to improve the accuracy of the numerical model of the actuator and the performance of the actuator under dynamic conditions and enable a precise control of its motion.

In the proposed method, only frequency is measured during the oscillation experiment; then, all the other mechanical quantities such as velocity, position, acceleration, and force are numerically calculated. In addition, force is directly calculated accord-

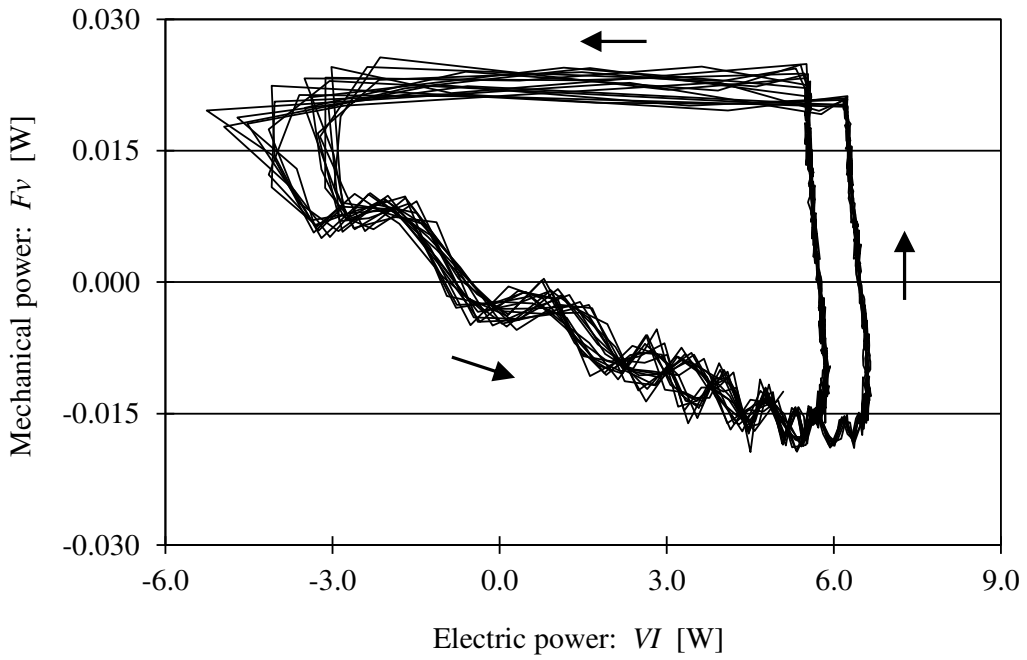

Figure 2.13: Relationship between electrical and mechanical power

ing to its definition, that is, the product of mass and acceleration.

2.2.4 Conclusions

A novel method for evaluating the electrical and mechanical characteristics of a voice coil actuator is proposed based on the LMM. Using the proposed method, the electrical and mechanical characteristics of a voice coil actuator are accurately determined and force transducers are not needed.

2.2.5 Future work

Recently, a miniaturized voice cell motor actuator is modified as an auto-focusing actuator. Therefore, a possible experiment for small size voice cell actuator is needed. In this case, a small size cube-corner prism or mirror can be used to instead of the moving part which used in section 2.2.

2.3 Method for evaluating the electro-mechanical characteristics of a piezo-electric actuators

2.3.1 Introduction

Piezo-electric (PZT) actuator, with high stiffness, compact size and high resolution, has been applied in many areas related to precision position and force control and measure [59–61]. The static output characteristics of conventional PZT actuator are typically evaluated by standard static methods, e.g., using static weights under static conditions. The dynamic outputs of PZT actuator including force and displacement are usually measured by using force and displacement transducer, respectively. However, so far, no standard dynamic calibration method for force transducer has been proposed. Instead of force transducer, a spring-mass-damper is used for dynamic analysis the characteristics of actuators [62, 63]. The dynamic force is measured as the impedance interactions between actuators and load structure, i.e., spring-mass-damper. In this method, the stiffness of spring and the coefficient of piezoelectric thin film stocked in actuator during motion direction are considered constant. However, compound components such as piezo-stack actuators cannot be described sufficiently by piezoelectric coefficients, which vary with temperature, pressure, electric field, mechanical and electrical boundary conditions etc. [64, 65]. A mass was loaded to PZT actuator by using a rotating arm via a high stiffness transmission rod [66]. Several displacement transducers were used to measure the rotation of the arm in order to calculate the force generated or applied on PZT actuator. In this device, the accuracy of displacement measurement is sensitive to temperature. Some models for the dynamic analysis of the electro-mechanical characteristics of PZT actuator are proposed [67, 68]. In those models, the design of mechanical parameters is based on testing actuator with dead weight, known structure or transducer etc. Several kinds of interferometer, such as signal frequency interferometer, laser Doppler interferom-

eter and laser diode interferometer etc., are introduced to accurately measure the displacement of actuators and piezoelectric thin film [69, 70]. However, they failed to measure the dynamic force.

This section aims to measure and evaluate the electric-mechanical characteristics of piezo-electric actuators during dynamic condition based on LMM. The method proposed in this section does not need any force transducer and the characteristics of host or preloading. Our method, the modified LMM, is different from the conventional Doppler velocimeter. First, in the LMM, the inertial force is measured as the definition of force, the product of mass and acceleration. Second, the beat frequencies of the laser lights are highly accurately calculated by the Zero-crossing Fitting Method (ZFM) [31]. All other quantities, e.g., velocity, acceleration, displacement and force, are calculated from the frequencies. In this section, a corner-cube prism (CC) is attached to the tip of PZT actuators with high stiffness metal blocks. The force generated by the actuator is calculated as the inertial force of the total mass of CC and blocks. A laser Doppler interferometer is introduced to measure the Doppler frequency shift caused by the motion of PZT actuators. Velocity, acceleration, force, power and displacement of the actuators during motion are measured from the Doppler frequency. Force-displacement behaviors of the actuators under dynamic condition are evaluated. The relationships of energy conversion between electrical and mechanical domains are also evaluated based on the observed results.

2.3.2 Experimental setup

A schematic diagram of experimental setup and photographs of measurement system are shown in figures 2.14 and 2.15, respectively.

A CC is attached to a piezo-stack actuator with some metal blocks and the total mass of metal blocks including the CC is 9.07 g. The actuator is driven by a sinusoidal signal at a frequency of 100 Hz which is generated by a function generator and amplified by a piezoelectric driver. The actuator is connected with a shunt resistor. The

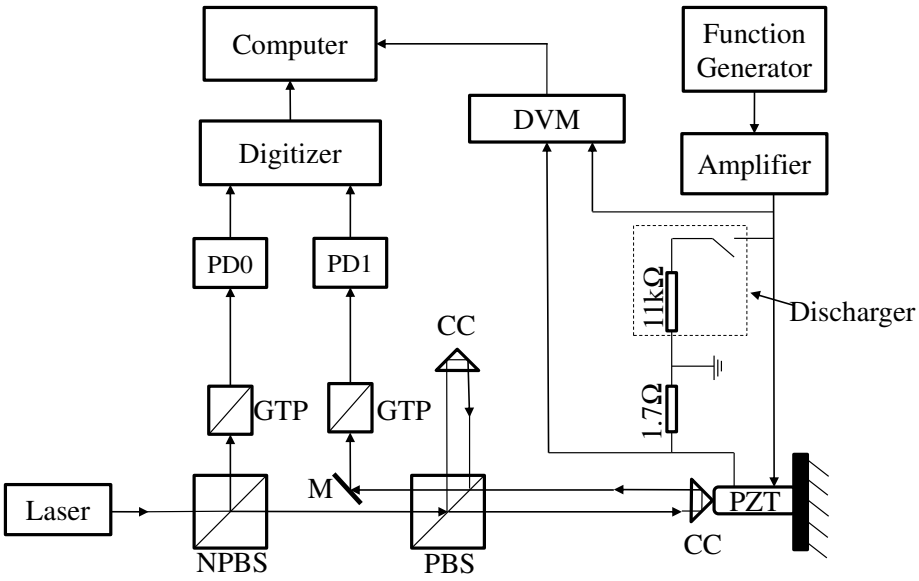

Figure 2.14: Experimental setup for evaluating the electro-mechanical characteristics of PZT.

voltage of actuator and shunt resister are measured by a digital voltmeter (DVM), which is based on a data acquisition card (PCI-6221, manufactured by National Instruments Corp., USA). The current of actuator is calculated as the current of shunt resistor. A discharger is used for discharging the actuator.

A Zeeman-type two-frequency He-Ne laser is used as the light source of the laser Doppler interferometer. The interferometer has two photo-detectors: PD0 and PD1. The waveforms appearing at PD0 and PD1 are recorded using a digitizer (model: 5102; manufactured by National Instruments Corp., USA) with the sampling rate of 20 MS/s and the sampling length of 5 M, then the frequencies are accurately calculated from the waveform using ZFM, in which all the zero-crossing are used for estimating the frequency in each measurement period [31].

The frequency difference, f_{rest}, between the two orthogonal polarization states light emitted from the laser is monitored using a Glan–Thompson prism (GTP) and PD0. The total force, F, acting on the attached mass is calculated as the product of

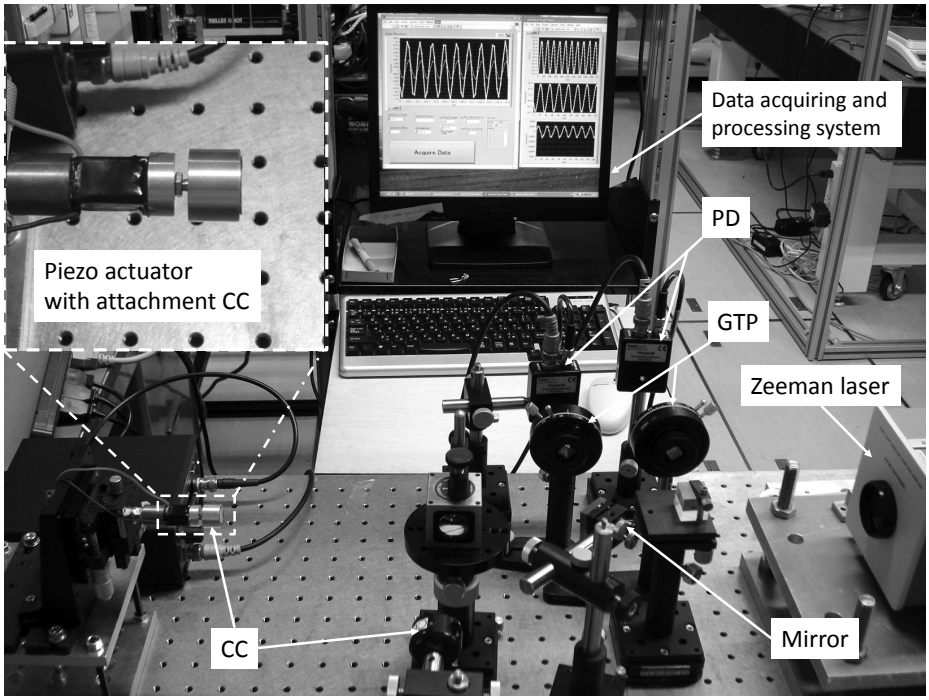

Figure 2.15: Photographs of measurement system.

its mass M and acceleration a as follows:

$$F = Ma \tag{2.12}$$

In the measurement, F is considered to be generated by the actuator and applied to the mass at the contact surface between the actuator and the mass. The acceleration is calculated from the velocity of mass which is measured as the Doppler shift frequency $f_{Doppler}$.

$$v = \lambda_{air} f_{Doppler}/2 \tag{2.13}$$

$$f_{Doppler} = f_{rest} - f_{beat} \tag{2.14}$$

where λ_{air} is the wavelength of the signal beam under the experimental conditions, and f_{beat} that appeared at PD1 is the beat frequency, which is the frequency difference between the signal beam and the reference beam. The direction of the coordinate

system for the velocity, acceleration and force is toward the right in figure 2.14. Its origin is set to be the center of movement of the actuator. All the other mechanical quantities, such as the position, acceleration and force of the mass, are numerically calculated from the velocity.

2.3.3 Zero-crossing fitting method

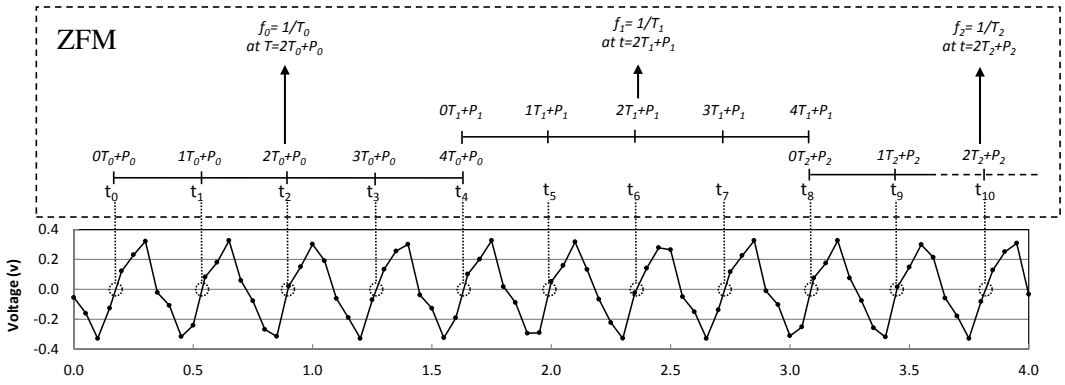

Figure 2.16: Algorithm of zero-crossing method (periods N=5).

Zero-crossing fitting method (ZFM) has been proposed by Y. Fujii for estimating frequency form the zero crossing times of the digitized waveform [31], as shown in figure 2.16 . To apply the ZFM, a harmonic model function is divided into segments by a factor N which indicates the periods of waveform, each characterized by its period T_j and phase $2\pi P_j/T_j$. The difference between the zero crossings time t_k of the model function and the sampled signal is given as:

$$C_j(T_j, P_j) = \sum_{i=0}^{N-1} \left[t_{i+j(N-1)} - (iT_j + P_j) \right]^2 \tag{2.15}$$

Then equation (2.15) can be minimized in the least–square sense by varying all $\{T_j\}$

and $\{P_j\}$ independently of each other.

$$\begin{cases} \dfrac{\partial C}{\partial T_j} = 2\sum\limits_{t=0}^{N-1}\left[t_{i+j(N-1)} + (iT_j + P_j)\right]^2(-i) \\ \dfrac{\partial C}{\partial P_j} = 2\sum\limits_{t=0}^{N-1}\left[t_{i+j(N-1)} + (iT_j + P_j)\right]^2(-1) \end{cases} \tag{2.16}$$

Set:

$$\frac{\partial C}{\partial T_j} = \frac{\partial C}{\partial P_j} = 0 \tag{2.17}$$

Then we can get:

$$\begin{aligned} &\frac{N(N-1)(2N-1)}{3}T_j + N(N-1)P_j = 2\sum_{i=0}^{N-1} it_{t+j(N-1)} \\ &N(N-1)T_j + 2NP_j = 2\sum_{i=0}^{N-1} t_{t+j(N-1)} \end{aligned} \tag{2.18}$$

From equation (2.18), the frequency can be obtained.

$$f_j = \frac{1}{T_j} = \frac{N(N-1)(N+1)}{12\sum\limits_{i=0}^{N-1} it_{i+j(N-1)} - 6(N-1)\sum\limits_{i=0}^{N-1} t_{i+j(N-1)}} \tag{2.19}$$

Thus, for each interval j containing N zero crossing times t_k $(k = 0, 1, 2 \ldots N)$ of the sampled signal, the frequency can be calculated from equation (2.19)

2.3.4 Results

Three PZT actuators with difference size named as P1, P2 and P3 shown in Table 2.1 are tested by the above mentioned experimental setup. All the actuators are discharged before tested. In the figures hereinafter shown, the data set obtained from the experiment of 0.1 s is shown. Since the driven signal and data processing for three actuators are same, figure 2.17 only shows the mechanical and electrical quantities of P1, which are measured by using our experimental setup. Figure 2.17(a) shows the frequencies f_{rest}, f_{beat} and the other mechanical quantities, such us velocity,

Table 2.1: Specification of PZT actuators P1, P2 and P3.

Name	**Dimensions**	**Displacement(100V)**	**Capacitance**
P1	10 ×10 ×18 mm	15 μm	6.59 μF
P2	6.5 × 6.5 ×18 mm	15 μm	1.6 μF
P3	3.5 × 4.5 ×10 mm	9.1 μm	0.18 μF

acceleration, force, mechanical power and displacement of actuator P1, calculated from the frequencies. The mechanical power is calculated as the product of force and velocity. Figure 2.17(b) shows the electrical quantities, voltage, current and electric power applied on P1. Usually, PZT actuator is considered as a capacitance load [73,74]. While, the phase difference between voltage and current is approximately 80.9° in figure 2.17(b). This is because the phase difference is influenced by the back-emf, due to the hysteresis [75, 76].

The relationships between the instantaneous mechanical power M_p and instantaneous electrical power E_p of P1, P2 and P3 (from left-to-right) are shown in figure 2.18. The regression lines of P1, P2 and P3 are:

- P1: $M_p = 4.4 \times 10^{-6} E_p - 7.27 \times 10^{-11}$,
- P2: $M_p = 1.56 \times 10^{-5} E_p + 5.53 \times 10^{-11}$,
- P3: $M_p = 1.24 \times 10^{-3} E_p + 1.4 \times 10^{-9}$.

The results show that small size of actuator can transform electric power into mechanical power more effectively. The efficiency of converting average power of electrical (E_{ave}) power to mechanical (M_{ave}) power of P1, P2 and P3 (M_{ave}/E_{ave}) are 4.8×10^{-7}, 7.25×10^{-6} and 8.63×10^{-5}, respectively. Most of the electric energy seems to be dissipated in the form of heat.

Figure 2.19 shows a set of figures of voltage and current against displacement and force of the three actuators. These figures show that the hysteresis of the PZT

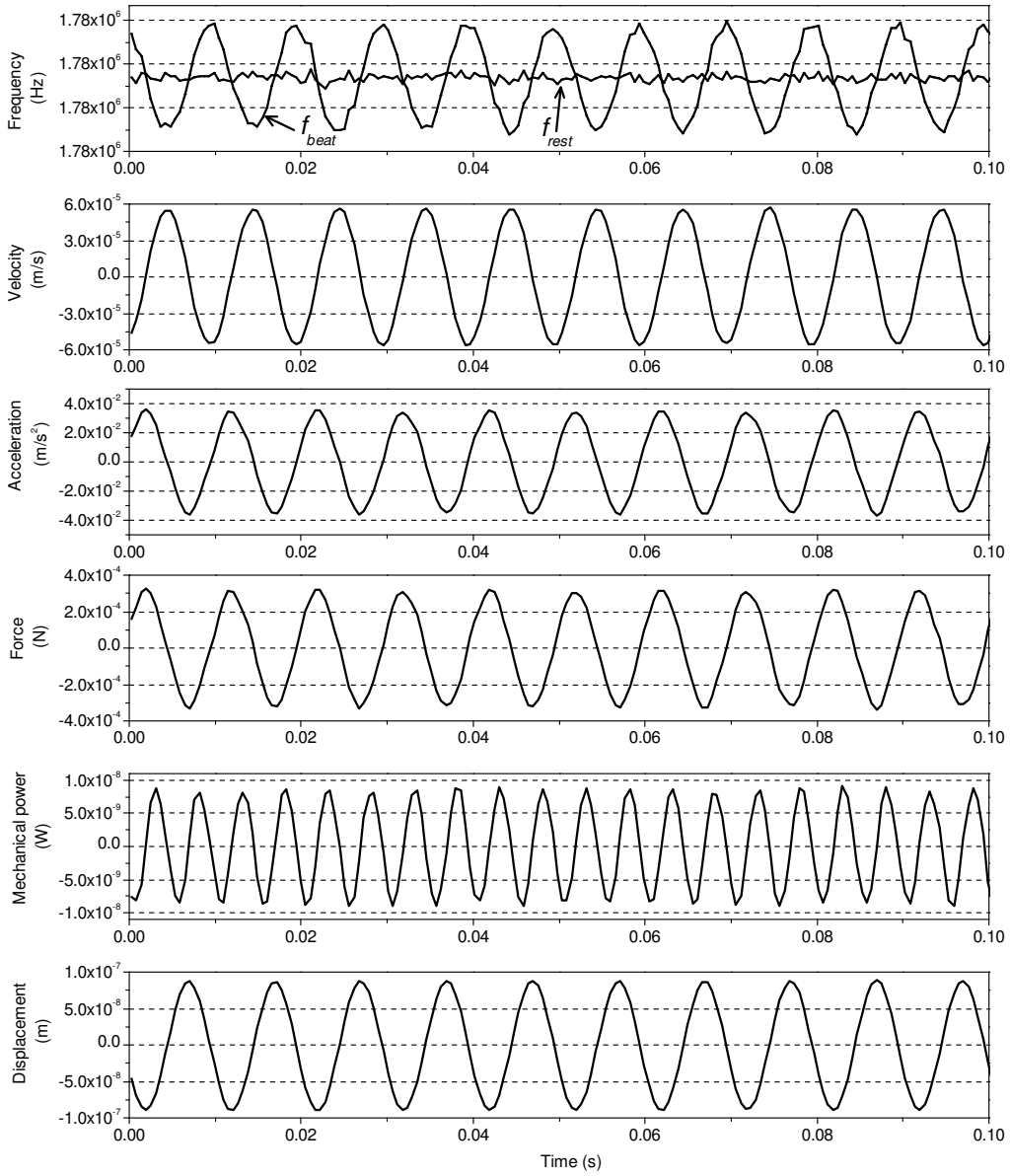

(a)

Figure 2.17: (**a**) The frequency of beat and rest laser beam, and mechanical quantities of PZT actuator P1; (**b**) The electrical quantities of PZT actuator P1.

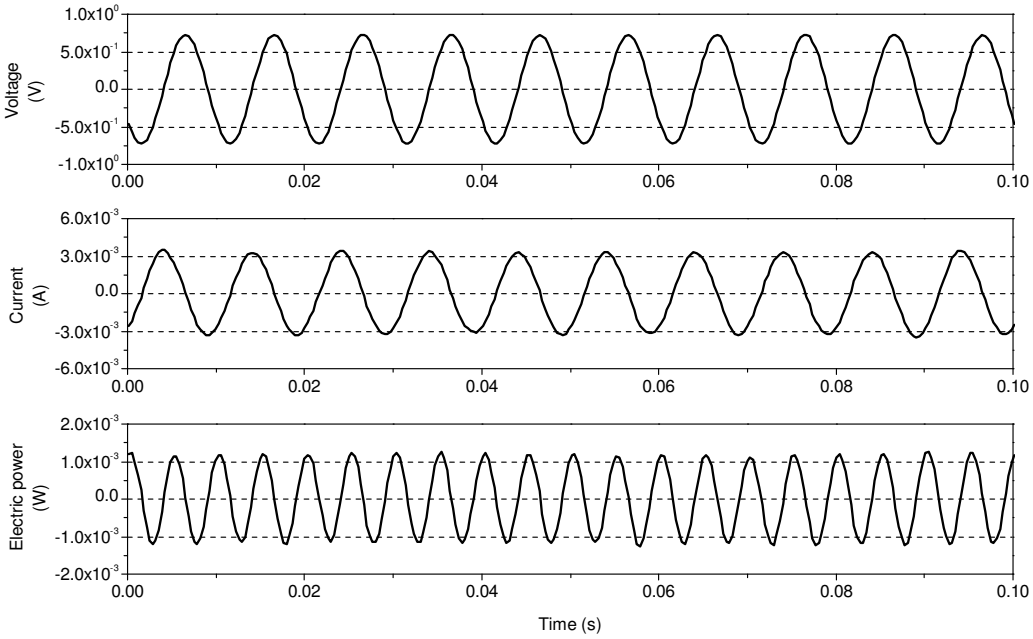

(b)

Figure 2.17: *Cont.*

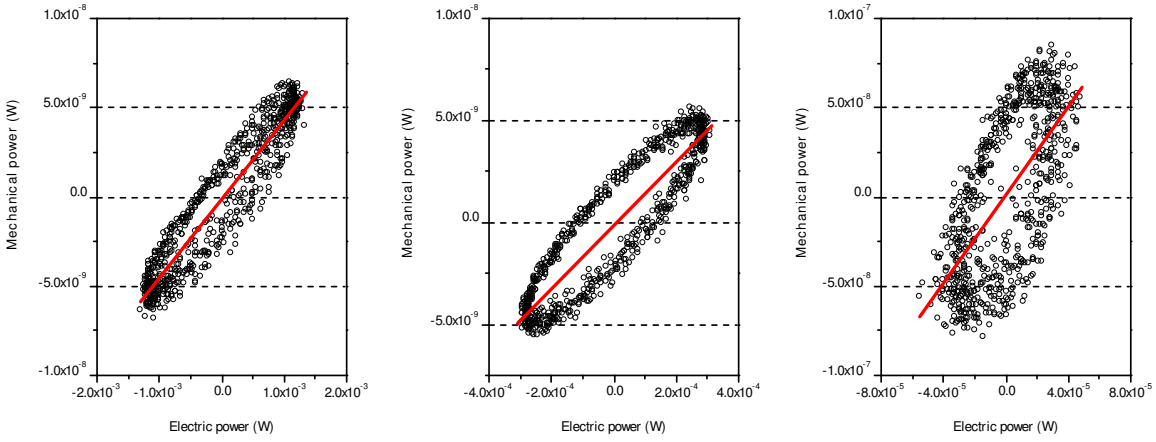

Figure 2.18: The instantaneous mechanical power changed against instantaneous electric power of P1, P2 and P3 from left to right.

actuators caused by voltage is larger than current. Particularly, the long length in the axial direction causes large hysteresis as shown in figure 2.19(a,c). The high reproducibility of data indicates that the hysteresis loops are congruent due to the input variation within the same range.

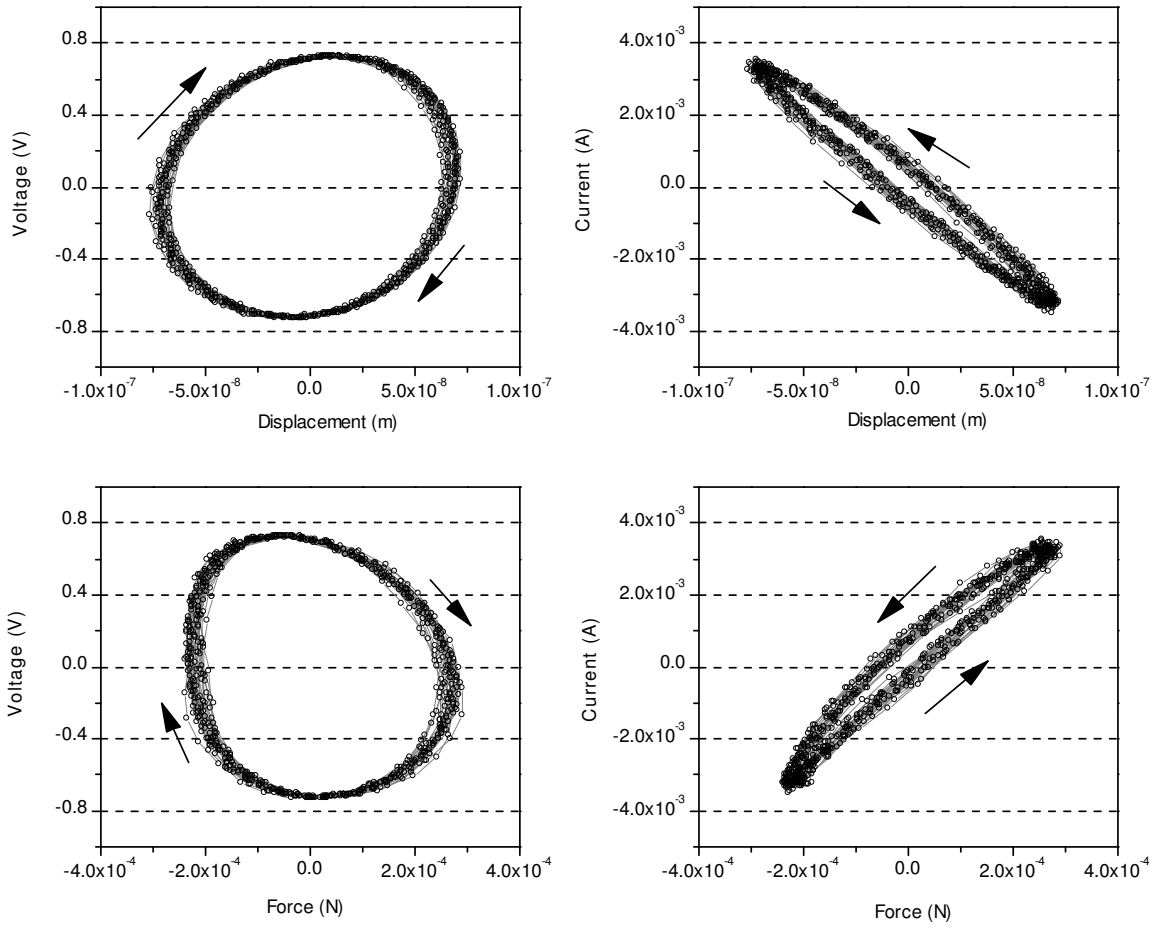

(a)

Figure 2.19: Voltage and current applied on the actuator, against displacement and force;
(**a**) P1; (**b**) P2 and (**c**) P3.

Figure 2.20 shows the velocity and force against displacement of the actuators P1, P2 and P3. Ten periods of reciprocating motion are recorded during this experiment. The reproducibility of data is very high during reciprocating motion. The regression

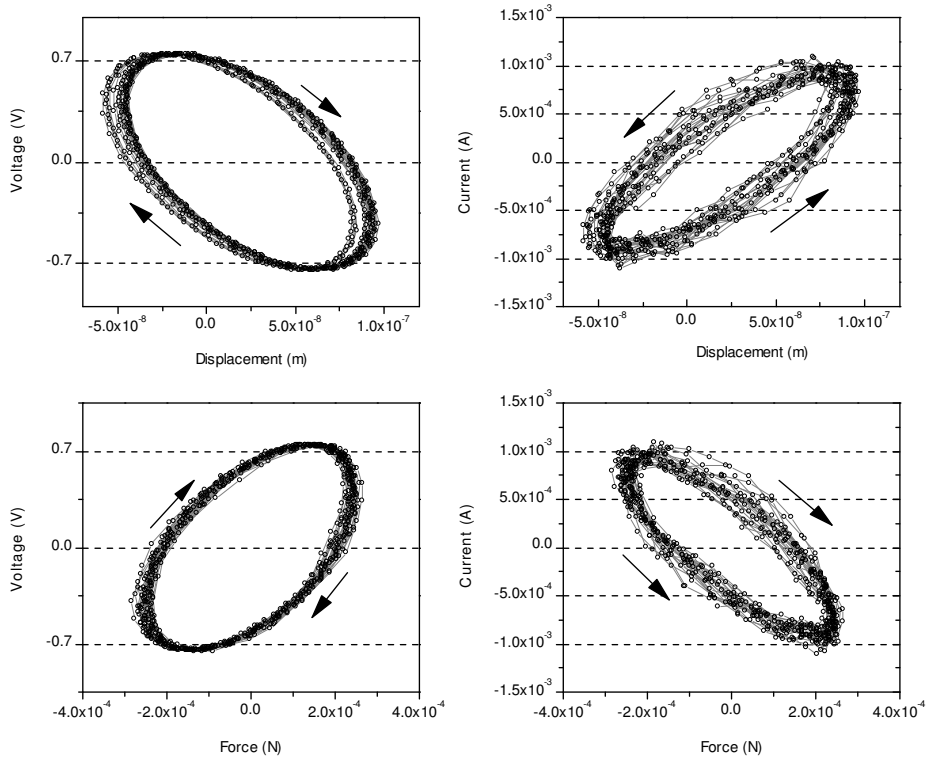

(b)

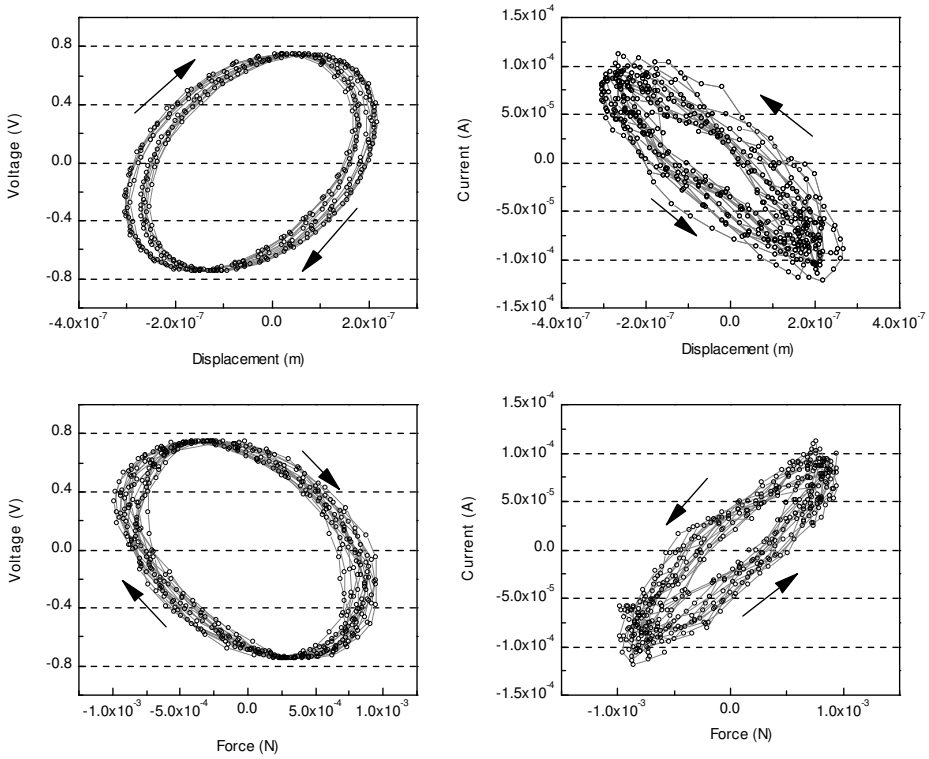

(c)

Figure 2.19: *Cont.*

line of force F against displacement x is:

$$\begin{aligned} \text{For actuator P1:} \quad F &= -3.56 \times 10^3 x + 3.02 \times 10^{-7} \\ \text{For actuator P2:} \quad F &= -3.54 \times 10^3 x + 7.35 \times 10^{-5} \\ \text{For actuator P3:} \quad F &= -3.49 \times 10^3 x - 1.15 \times 10^{-4} \end{aligned}$$

From Figure 2.20, the actuators can be regarded as a spring with spring constant about 3.56×10^3 N/m of P1 (k_{p1}), 3.54×10^3 N/m of P2 (k_{p2}) and 3.49×10^3 N/m of P3 (k_{p3}). In sinusoidal operation, the spring constant k can be concluded as: $k = 4\pi^2 m_{eff} f^2$ from manufacturer, where f is the operation frequency, m_{eff} is the effective mass which relates to the loading and measuring point [65]. If the measuring point is assumed at the tip of PZT actuator, then m_{eff} is considered as the mass of attachment, and k is equal to 3.58×10^3 N/m, which is 0.56% higher than k_{p1}, 1.12% higher than k_{p2} and 2.58% higher than k_{p3}. It may be because the measuring point where the acceleration is measured by interferometer is not equal to the tip of PZT actuator. In other words, this error may be caused by the mass between the tip of PZT actuator and the measuring point. The correlation coefficients of the fitting line in figure 2.20 are higher than 0.9, indicating a very well linear relationship between force and displacement generated by the actuator.

Using the proposed method, the electro-mechanical characteristics of PZT actuators which are being driven can be measured easily and accurately. Force, which acts on the mass attached to the actuator under test, is measured as the inertial force of the mass itself, *i.e.*, $F = Ma$. This is the most significant compared with other conventional methods. In this section, only three sizes of stack piezo-stack actuators are tested. However, the developed method can be easily applied to evaluate the dynamic characteristics of different type of actuators and to evaluate the actuator driven by different types of excitation (e.g., changing the waveform, frequency or amplitude of the drive signal). This experiment is also able to calibrate actuators and estimate a mass whose inertial force can be measured by the calibration using the actuators.

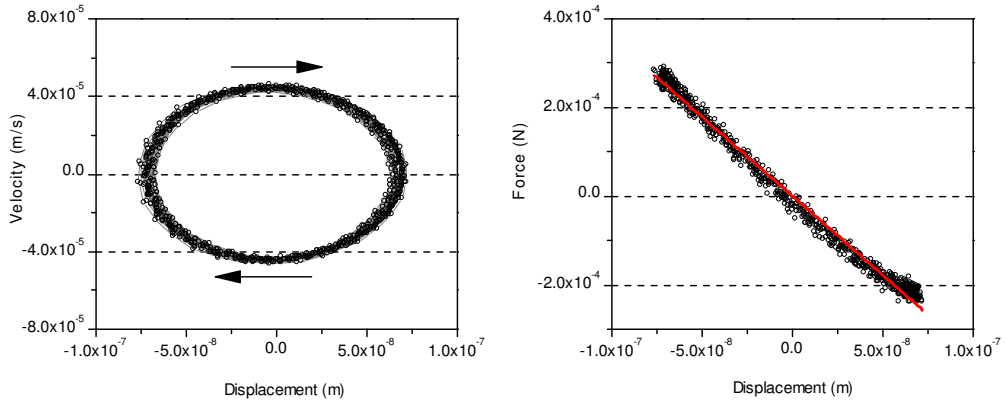

(a)

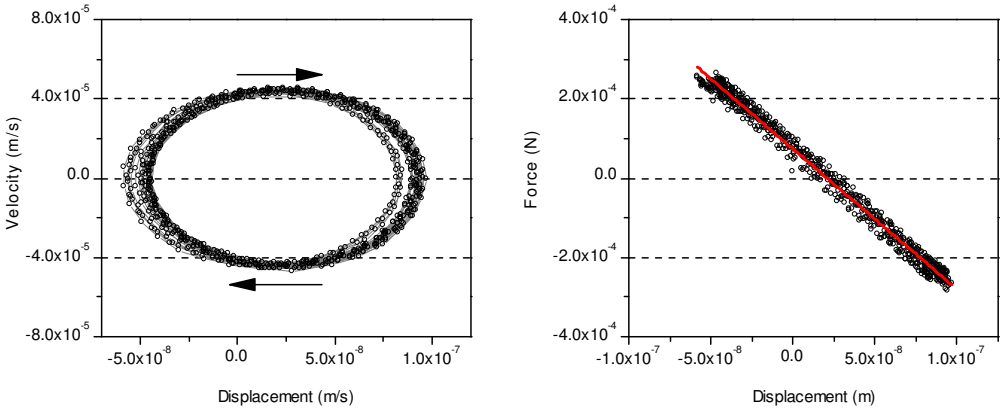

(b)

Figure 2.20: Velocity and force changed against displacement; (**a**) P1; (**b**) P2 and (**c**) P3.

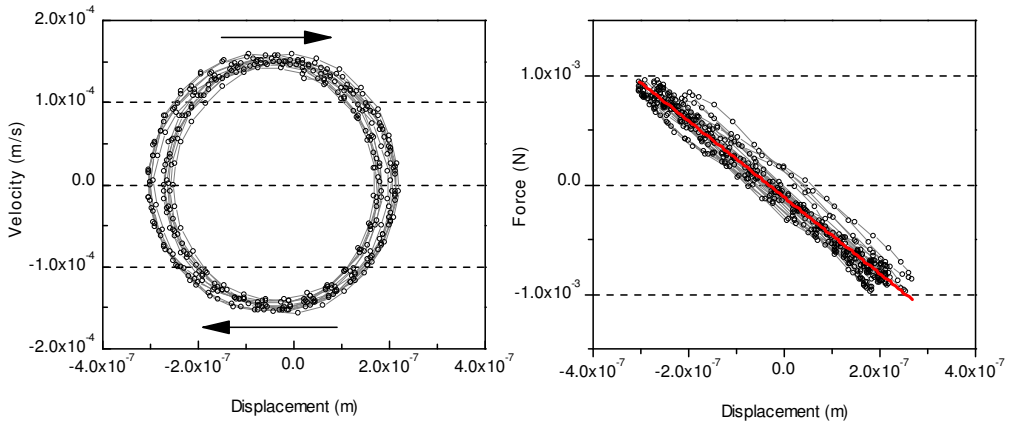

(c)

Figure 2.20: *Cont.*

Precision measurements of the electrical and mechanical characteristics of the actuator should contribute to understanding the mechanism of the actuator and realizing more precision controllability of the actuator.

2.3.5 Discussion

Piezoelectricity involves the interaction between the electrical and mechanical behavior of the material. This interaction has been approximated by static linear relations between two electrical and mechanical variables 2.20:

$$\mathbf{S} = \mathbf{s}^E\mathbf{T} + \mathbf{dE}$$

$$\mathbf{D} = \mathbf{dT} + \varepsilon^T\mathbf{E} \tag{2.20}$$

where $\mathbf{S}$ is a strain tensor, $\mathbf{T}$ is a stress tensor, $\mathbf{E}$ is an electric field vector, $\mathbf{D}$ is an electric displacement vector, $\mathbf{s}^E$ is an elastic compliance matrix when subjected to a constant electric field (the superscript E denotes that the electric field is constant), $\mathbf{d}$ is a matrix of piezoelectric constants and ε^T is a permittivity measured at a constant stress.

The piezoelectric effect is, however, very non-linear in nature. Piezoelectric materials exhibit for example a strong hysteresis and drift that is not included in the above model. Figure 2.19 also shows that the hysteresis caused by voltage is larger than by current. It's reasonable because, when connected electrically, the actuator acts like a non-linear capacitor which changes its capacitance even when the input voltage is kept constant. In order to remove the hysteresis, some methods such as voltage driver, charge driver and capacitor insertion method are used. The advantage and disadvantage of these three methods are listed as following:

1. For voltage driver: it's easy to use and does not reduce the operating range and bandwidth of a piezoelectric actuator. However, it comes with the disadvantage of having to cope up with hysteresis and creep. This affects precise positioning while using a piezoelectric actuator.

2. For charge or current driver: it's easy to remove the hysteresis and get linear control. However, the simplicity of such linear control is bought at the expense of the increased electronic complexity required for effective charge control.

3. For capacitor insertion method: it's easier than using charge driver method. The piezoelectric actuator's characteristics become more linear by using this method. While, the reason behind this method is the requirement of higher voltage input.

2.3.6 Conclusions

A precision method for evaluating the electrical and mechanical characteristics of actuators is proposed and demonstrated by evaluating the characteristics of three PZT actuators with difference size which are being driven. The main feature of the proposed method is that only two physical quantities are needed to be measured. One is Doppler frequency shift and the other is mass. Compared with traditional methods, force transducer, displacement transducer and known load structure are

not needed in this method. This method will be useful for better understanding the dynamic characteristics of PZT actuators during motion and for precisely controlling its position under dynamic conditions.

2.3.7 Future work

In the future, a three-dimensional measurement of the PZT actuator is needed. The three dimensional measurement of the actuator can be realized by means of introducing three interferometers with three signal beams, which are not in the same plane and introduced to the CC attached to the actuator. Each signal beam has the sensitivity only for the component of the movement of the optical center (OC) of the CC of the signal beam's direction. If the gravity center (GC) of the attached mass coincides with the OC of the CC, then the force component along each signal beam can be calculated as the product of the mass and the acceleration of the OC along the direction of each signal beam.

2.4 High speed tester

2.4.1 Introduction

For studying and evaluating the properties of materials under dynamic loading conditions, the levitation mass method (LMM) has been used [54, 56, 71, 77–80]. In the LMM, the inertial force is calculated as the product of mass and acceleration which is measured using a dual-frequency (f_1, f_2) laser Doppler interferometer. While, in forth and back motion, the measurable velocity of interferometer is limited at the critical velocity $v_c = \lambda|f_1 - f_2|/2$. In order to obtain high measurable velocity, interferometer including an acousto-optic modulator [81] or two frequency laser system utilizing the birefringent effect is used [82]; and a birefringent dual frequency He-Ne laser is developed to get frequency difference range from zero to several hundred MHz [83]. However, these methods increase the complexity of optics and their costs.

Y. Fujii has developed a dual beat-frequencies laser Doppler interferometer (DB-LDI) with low frequency difference laser for measuring the high velocity in forth and back motion [84]. In DB-LDI, two laser beams with difference frequency are both used as reference and signal beams which compose two beat signals. Although the velocity calculated from one of the beat frequencies reaches critical velocity, the velocity calculated from the other beat frequencies is far from critical velocity. Therefore, by using this interferometer, the high velocity in forth and back motion can be measured.

In this section, a high-speed impact testing method for evaluating materials is proposed. An inertial mass as a moving part is levitated using an aerostatic linear bearing. The mass is collided with a material under test by given a high initial velocity. The velocity of the mass which is even higher than the critical velocity before and after collision is measured by DB-LDI from Doppler frequency shift. Subsequently, the position, acceleration and impact force of the mass and the mechanical hysteresis and energy consumption of the material during the collision are evaluated.

2.4.2 Principle of dual beat-frequencies laser Doppler interferometer

Figure 2.21 shows a schematic of a dual beat-frequencies laser Doppler interferometer (DB-LDI). The light source is a Zeeman-type two-frequency He-Ne laser, which generates a pair orthogonally polarized laser light at two frequencies with a difference $f_{rest} = (f_1 - f_2)$, where f_1 and f_2 are the frequencies of laser lights and $f_1 > f_2$. The two beams are both divided into reference beams and signal beams by a non-polarized beam splitter. The reference beams are returned by a corner-cube prism (CC1) with their polarization rotated by a quarter-wave plate. Finally, the reference beams are divided at each frequency by a polarized beam splitter (PBS). f_1 is introduced into a photodetector (PD1), and f_2 is introduced into the other photodetector (PD2). The signal beams are returned by CC2 with their frequencies modulated by Doppler shift. The modulated beams, $f_1^{'}$ and $f_2^{'}$ are divided by the PBS. $f_2^{'}$ is introduced into PD1, while $f_1^{'}$ is introduced into PD2. Therefore, each PD detects a beat signal, $f_{beat1} = |f_1 - f_2^{'}|$ and $f_{beat2} = |f_1^{'} - f_2|$, respectively.

The frequencies of the signal beams modulated by Doppler shift are described as:

$$f_1^{'} = f_1 - f_{Doppler} \tag{2.21}$$

$$f_2^{'} = f_2 + f_{Doppler} \tag{2.22}$$

$$f_{Doppler} = -2v/\lambda \tag{2.23}$$

where λ is the wavelength of the laser and v is the velocity of CC2.

Figure 2.22 shows the calculated relationships between the velocity and beat frequencies when $f_{rest} = 1.76$ MHz and $\lambda = 632.9$ nm. In the case of laser Doppler velocimetry using a single beat signal, which is the conventional method, v is calculated using the following equation:

$$\begin{aligned} v &= \frac{\lambda}{2}(f_{beat1} - f_{rest}) \\ &= -\frac{\lambda}{2} f_{Doppler} \end{aligned} \tag{2.24}$$

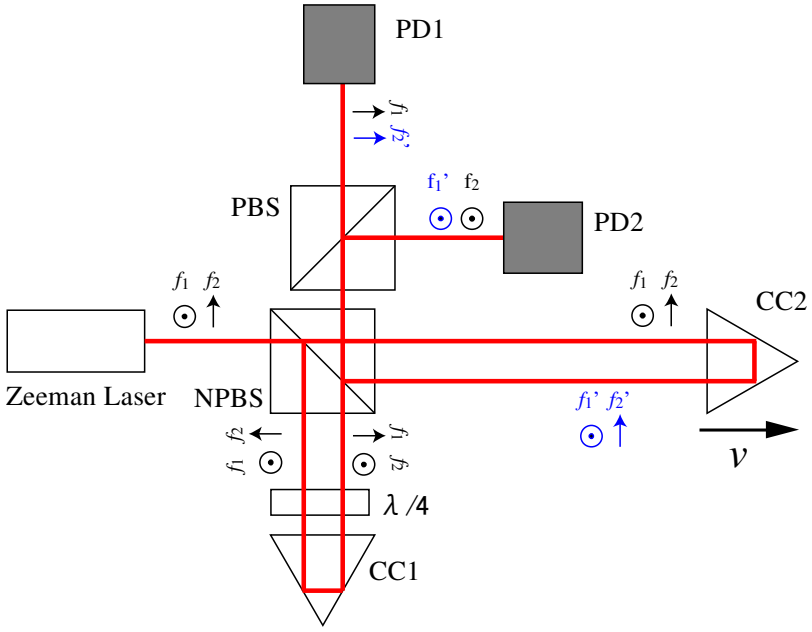

Figure 2.21: Schematic of dual beat-frequencies laser Doppler interferometer (DB-LDI).

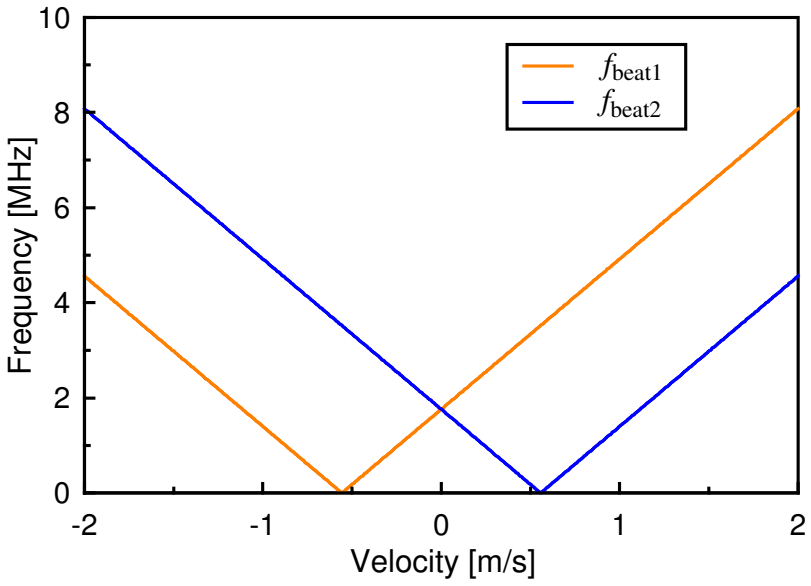

Figure 2.22: Relationships between velocity and f_{beat1} and f_{beat2}.

When v is below a critical velocity, $-v_c = -\lambda f_{rest}/2 = -0.56$ m/s, the velocity calculated from f_{beat1} is not correct. Because $|f_1 - f_2^{'}|$ is positive even though $(f_1 - f_2^{'})$

becomes negative. The same problem occurs for f_{beat2} when $v > v_c$. $-v_c$ is lower limitation for v for using f_{beat1} and v_c is upper limitation for v for using f_{beat2}. This is a serious problem for measurement of back and forth motion using a single beat signal. To overcome this problem, both f_{beat1} and f_{beat2} are used.

In the velocity calculation step, f_{beat1} and f_{beat2} are used to detect whether v reaches upper or lower limitation. Then, v can be calculated from f_{beat1} and f_{beat2} as follows:

(a) Calculate using f_{beat1}

$$v_1 = \begin{cases} \frac{\lambda}{2}(f_{beat1} - f_{rest}) & (f_{beat1} - f_{beat2} > -2f_{rest}) \\ -\frac{\lambda}{2}(f_{beat1} + f_{rest}) & (f_{beat1} - f_{beat2} = -2f_{rest}) \end{cases} \tag{2.25}$$

(b) Calculate using f_{beat2}

$$v_2 = \begin{cases} \frac{\lambda}{2}(f_{beat2} + f_{rest}) & (f_{beat1} - f_{beat2} = 2f_{rest}) \\ -\frac{\lambda}{2}(f_{beat2} + f_{rest}) & (f_{beat1} - f_{beat2} < 2f_{rest}) \end{cases} \tag{2.26}$$

By using equation (2.25) and (2.26), the two velocities can be calculated using both f_{beat1} and f_{beat2}. The two velocities can be used to enhance the accuracy of the velocity of object by averaging the velocities, while the frequencies of both beat signals are inside the dynamic range of this method is limited only the dynamic range of the frequency measurement method. The dynamic range of this method is limited only the dynamic range of the frequency measurement method and it can be extended more easily than increasing the frequency difference of the laser.

2.4.3 Experimental setup

Figure 2.23 shows the experimental setup for an impact test with high impact velocity. A moving part levitated using an aerostatic linear bearing is used to generate impact force, when it is collided with the elastic material under test. A corner-cube prism (CC1) and some metal blocks for adjusting the colliding point are attached on the

moving part. The total mass M of this combination approximate 17.938 g is measured by using a commercial electronic scale. The inertial force as the product of mass M and acceleration a, i.e. $F_{inertial} = Ma$, is accurately measured by using DB-LDI.

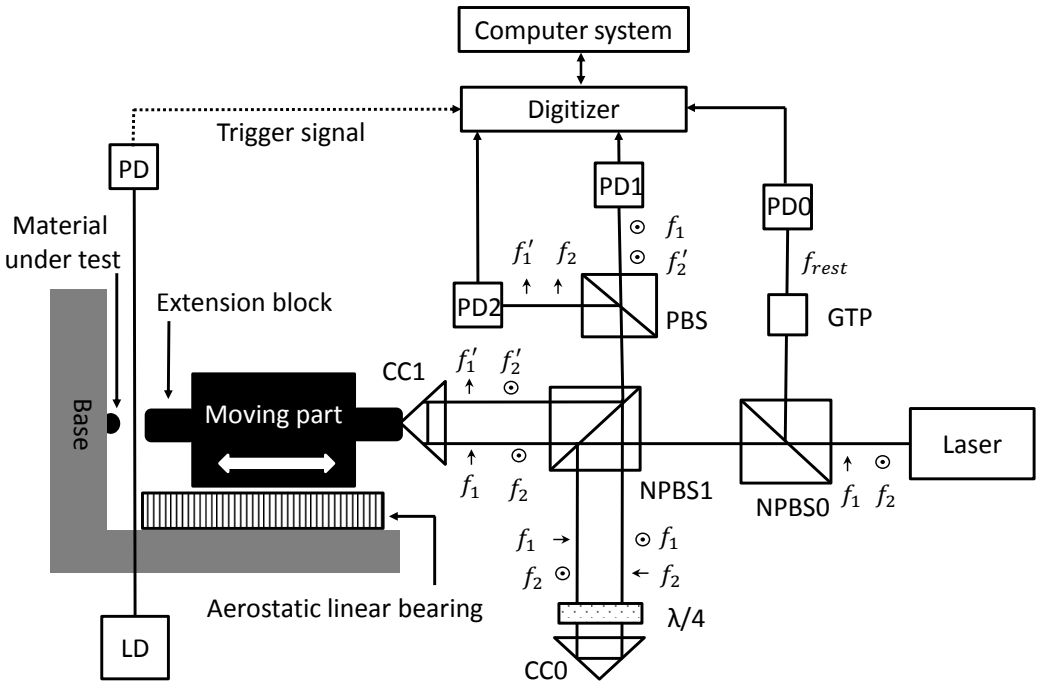

Figure 2.23: Experimental setup for testing material with high impact velocity.

In DB-LDI, the light source (HP5518A, Hewlett-Packard) generates a pair orthogonally polarized light beams at two frequencies (f_1, f_2) with a frequency difference $f_{rest} = f_1 - f_2$. The light from laser source is divided into two lights by a non-polarized beam NPBS0. One of them is detected by a photodetector (PD0) and the other is introduced to NPBS1. The two beams with difference frequencies are both divided into signal and reference beams by NPBS1. The reference beams are reflected by CC0 which is static and their polarized direction are rotated by a quarter-wave plate $\lambda/4$. The signal beams are reflected by CC1 and their frequencies are modulated by Doppler shift f_d, i.e. $f_1^{'} = f_1 + f_d$ and $f_2^{'} = f_2 + f_d$. The modulated beams and reference beams are divided into two interference beams by a polarized beam splitter (PBS) according to their polarized direction. The beat frequencies of interference

beams detected by detector PD1 and detector PD2 are named as f_{beat1} and f_{beat2}, respectively. A low-coast digitizer (NI 5102, by National Instruments Corp., USA) is used to record the intensity waveform of interference signals from PD0, PD1 and PD2 with sampling rate of 20 MHz and sampling length of 5 M for each channel.

The measurement system is triggered by a light switch which is composed by a laser diode and a photodetector. The impact force F is treated as the inertial force generated by the moving part, i.e. $F = Ma$, since the friction force between the moving part and an aerostatic linear bearing is small enough [56]. The acceleration is calculated from the velocity v of CC1 which is measured from Doppler frequency shift by DB-LDI by using equation (2.25) and (2.26).

2.4.4 Results and Discussion

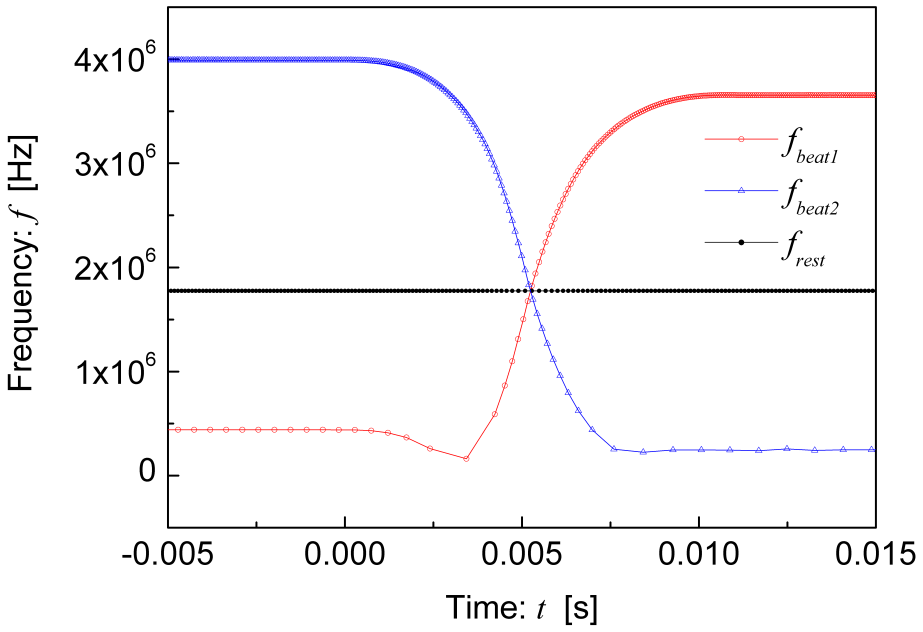

Figure 2.24: Frequencies of beat signals measured using dual beat-frequencies Laser Doppler interferometer.

The moving part is given a high initial velocity before triggering the experiment system. Figure 2.24 shows the frequencies, f_{beat1}, f_{beat2} and f_{rest}, measured using DB-LDI. These frequencies are calculated from the recorded digital waveforms of the interference signals by using a zero-crossing fitting method (ZFM) [31]. The rest frequency f_{rest} and the wavelength of the laser which we used are 1.77 MHz and 632.9 nm, respectively, therefore, the critical velocity is ± 0.56 m/s. As shown in figure 2.24, before the collision, the beat frequencies f_{beat2} and f_{beat1} are 3.99 MHz and 0.45 MHz, respectively. The Doppler frequency shift calculated from f_{beat2} is 2.22 MHz which is higher than 1.32 MHz calculated from f_{beat1}. It's because Doppler frequency shift is higher than rest frequency before colliding. In other words, the velocity of CC1 is lower than -0.56 m/s. After collision, the inertial mass moves back, the frequency f_{beat1} increases to 3.66 MHz and f_{beat2} decreases to 0.23 MHz. Doppler frequency shift calculated from f_{beat2} is lower than it calculated from f_{beat1}. That means the velocity of CC1 is higher than 0.56 m/s.

Figure 2.25 shows the velocity of CC1 calculated from single beat frequency f_{beat1} or f_{beat2}. It clear shows that the velocity of CC1 cannot be accurately measured when it higher or lower than critical velocity, $\pm v_c = \pm 0.56$ m/s, by using traditional single beat frequency laser Doppler interferometer.

Figure 2.26 shows the velocity v of CC1 which is calculated using v_1 and v_2. The velocity v is approximate -0.71m/s before collision and 0.60 m/s after collision, which is lower than $-v_c$ (0.56 m/s) and higher than v_c (0.56 m/s), respectively. The velocity v_1 and v_2 are calculated from Doppler frequency shift by using equation (2.25) and (2.26). As shown in figure 2.26, if only using v_1 or v_2, the time resolution of v is very low when the beat frequencies f_{beat1} and f_{beat2} near 0 Hz. While by using v_1 and v_2, the time resolution of v is very high.

Figure 2.27 shows the position, acceleration and impact force calculated from the velocity during the experiment. The origin of horizontal axis is set at the beginning of collision. Impact force F is considered as the inertial force of the moving part.

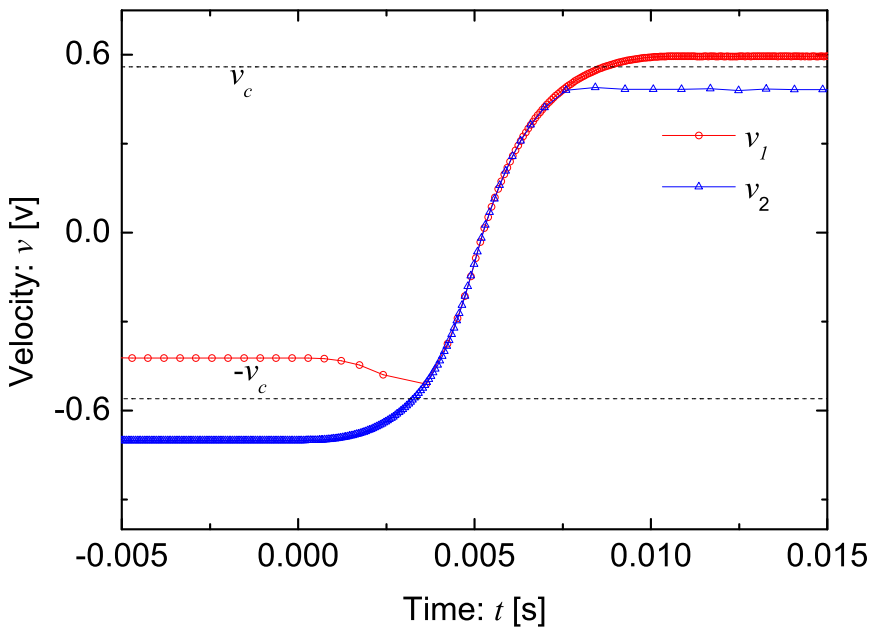

Figure 2.25: Velocity of CC1 measured using single beat frequency laser Doppler interferometer.

The maximum impact force applied on material is approximately 7.1 N when the acceleration arrives 396.5 m/s^2 as shown in figure 2.27 (b) and (c).

As shown in figure 2.28, the displacement of material changes approximately 2.81 mm during the collision. The elastic hysteresis of material is obtained in this experiment. The area of hysteresis loop is the energy dissipated due to material plasticity.

Figure 2.29 shows the force changing against velocity. The absolute value of velocity changed from 0.71 m/s to 0.60 m/s after collision due to material plasticity. The energy dissipates approximate 0.08 J during the collision, which is calculated as:

$$\Delta E = \int F \cdot v_{bef} \mathrm{d}t - \int F \cdot v_{aft} \mathrm{d}t$$

where v_{bef} and v_{aft} mean the velocity before and after collision.

The experiment results demonstrate the performance of the proposed method. In this method, the measurable velocity is not limited by the frequency difference of

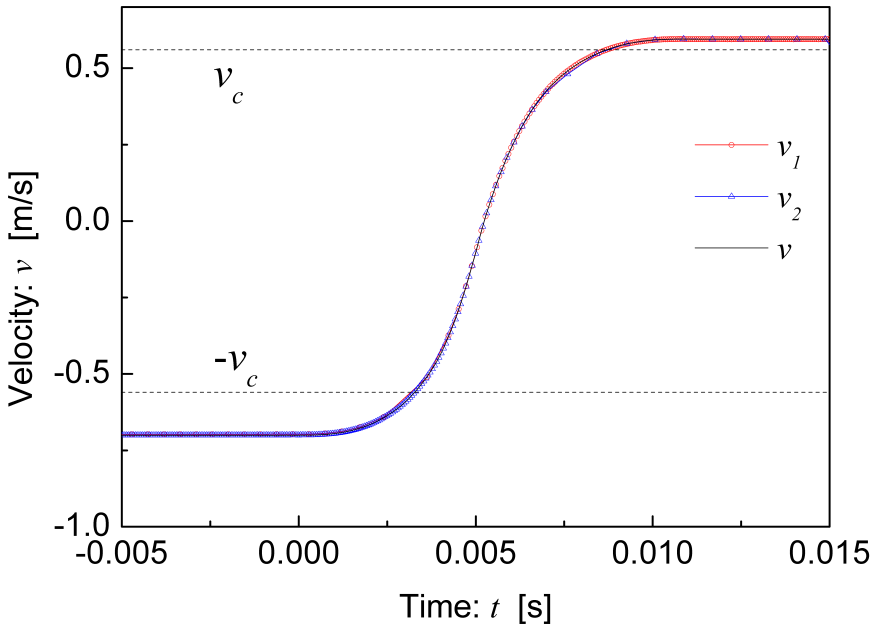

Figure 2.26: Velocity of CC1 measured using dual beat-frequencies laser Doppler interferometer

laser even the difference is low. By using this method, materials can be evaluated with high impact velocity using a low frequency difference laser based on LMM. In addition, this method also can be developed to test materials or structure under kinds of force such as step force and oscillation force by change the motion of the moving part.

2.4.5 Conclusions

This section presents a high-speed impact testing method for evaluating materials with high impact velocity. The material is collided by a levitated mass which is moved by giving a high initially velocity. The impact force is measured as the inertial force of the mass which is measured using a dual beat-frequencies laser Doppler interferometer. A low frequency difference laser is used as the light source of the

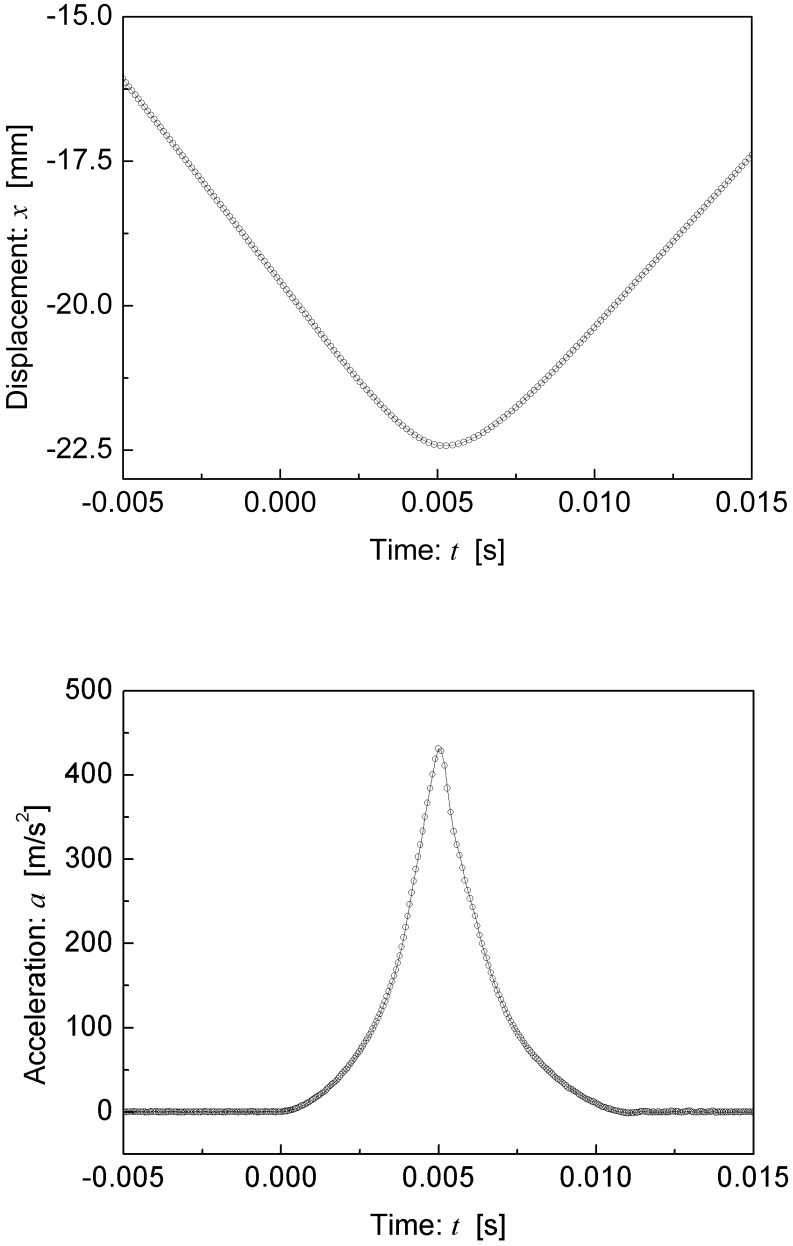

Figure 2.27: Position, acceleration and force calculated from velocity (a-c).

interferometer. During the collision, the Doppler frequency shift even higher than the frequency difference is accurately measured. Subsequently, the velocity, impact force, position, acceleration, mechanical hysteresis and energy dissipation of materials

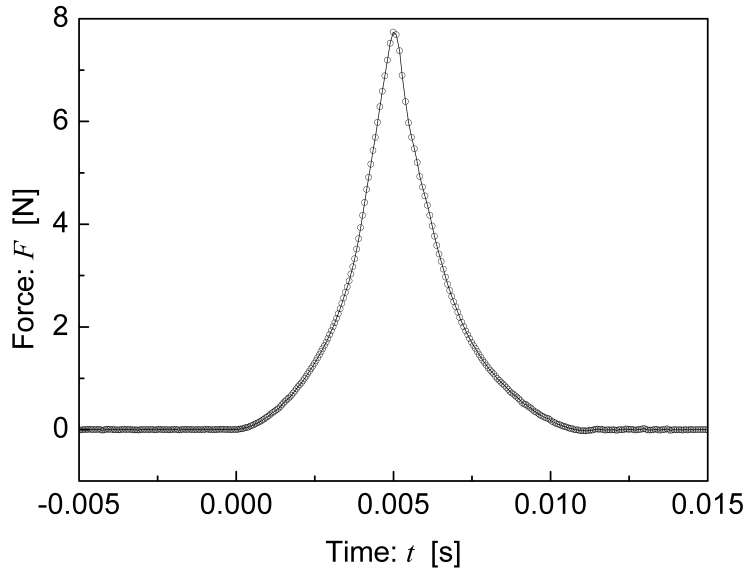

Figure 2.27: Position, acceleration and force calculated from velocity.

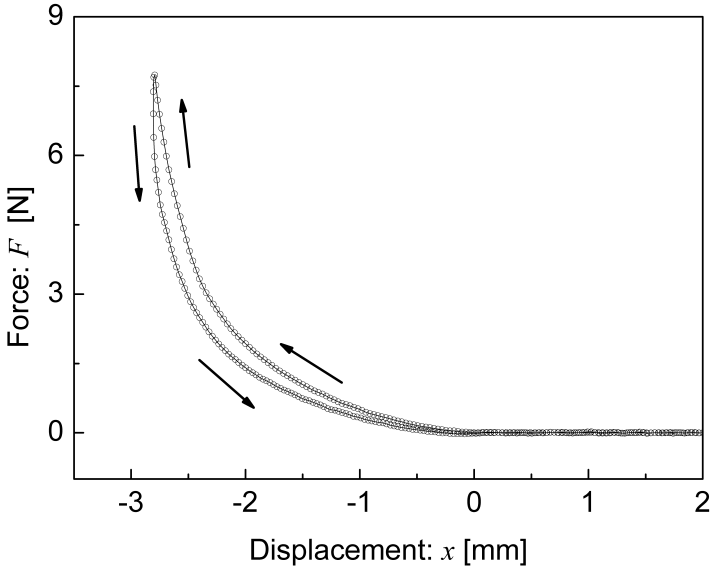

Figure 2.28: Force changing against displacement.

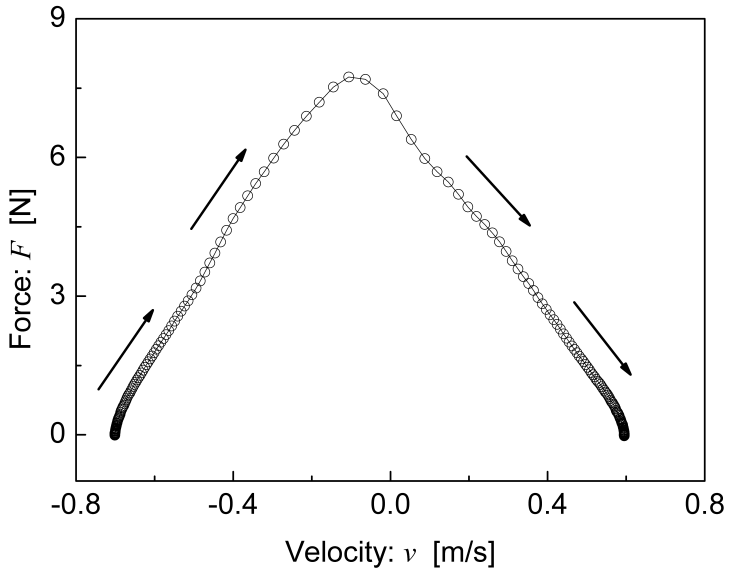

Figure 2.29: Force changing against velocity.

during collision are evaluated.

Table 2.2: Comparison of the methods for measuring high velocity.

Methods	Frequency difference	Measurable velocity
Acousto-optic modulator	$\sim$ 20 MHz	$\sim$ 5.1 m/s
Utilizing birefringence effect	40 MHz$\sim$1 GHz	12 m/s$\sim$300 m/s
Birefringence Zeeman laser	3$\sim$40 MHz	0.9 m/s$\sim$12 m/s
DB-LDI	no limitation of low or high frequency difference	not limited by the frequency difference

As shown in table 2.2, compared with other methods, by using DB-LDI, the mea-

surement method and experimental setup are more easier than using above-mentioned methods.

2.4.6 Future work

Based on the LMM and dual beat-frequencies laser Doppler interferometer, the materials can be tested with high collision velocity. Therefore, in the future work, we will try to testing the materials with typical force such as impulse and step force with high collision velocity. In this case, the spring and damping characteristics of the load mass may be needed to considered. It's because that the formula (1.1) is an ideal formula in the low frequency range. As the results shown in [85], the deviations increase rapidly when the frequency higher than 2 kHz.

Chapter 3

Conclusions and Future Prospects of the LMM

Levitation mass method is one of high-precision force measurement method developed by Y. Fujii. Due to its simple structure and high-precision, LMM has been modified to suit the dynamic force calibration of force transducers against some typical dynamic forces, such as impact force, step force and oscillation force. It's also used to evaluate the viscoelasticity of materials under impact load. Moreover, with a reference force, the mass of object can be estimated by using LMM. Based on the study of LMM, this thesis furthers the application of LMM, improves the property of laser Doppler interferometer and first proposes a new algorithm for calculating the acceleration. In this chapter, we summarize the key developments in this thesis and point out areas for future research.

3.1 Conclusions

Section 2.1 of chapter 2, the dynamic frictional characteristics and pitching angle of the linear ball bearings is precisely measured by using the LMM. In the measurement, two corner-cube prisms are attached to the difference points of the moving part which

is connected to the linear ball bearing. The results will help in understanding the mechanics of friction and in developing an improved method for the position control of linear actuators with linear bearings.

Section 2.2 and 2.3 of chapter 2 provide the methods for evaluating the electro-mechanical characteristics of a voice coil and a piezo-electric (PZT) actuator. While, the experimental devices for evaluating voice coil and PZT actuator are different.

1. For evaluating the voice coil, a moving part is connect to the coil. The force generated by coil is considered as the inertial force of moving part. In this case, the friction force of air bearing should be carefully considered.

2. For evaluating PZT actuator, a corner cube prism is attached on the top of actuator directly.

Section 2.4 of chapter 2 describes a high speed material tester. In this tester, the high inertial velocity which is given to moving part is accurately measured using a dual beat-frequencies laser Doppler interferometer (DB-LDI). In DB-LDI, two laser beams with difference frequencies are used to combine two beat signals. The measurable velocity is not limited by the frequency difference, even the frequency difference is low. Based on LMM, the mechanical characteristics of a material under test against impact force with high collision velocity are evaluated by using DB-LDI.

3.2 Future Prospects of the LMM

Also LMM is modified for dynamic calibration force transducer and material testing. The following areas are recommended for future research:

1. Expansion the testing range of force from 1 mN $\sim$ 1 kN.

2. Improving the accuracy of frequency estimation.

3. Testing materials in room temperature (from low to high temperature).

4. In order to remove the influence of atmosphere, putting the moving part in a vacuum environment.

Acknowledgements

I would like to express my sincere gratitude to all those who have advised me and help me through the completion of this thesis. This work would be impossible without their strong support in these years.

I'd like to express my sincere gratitude to my thesis and research advisor, Professor Yusaku Fujii. You passionately and patiently guided me through the entire research, and support me living in Japan. Without your immeasurable help, I wouldn't even have been able to start this work.

I am grateful for the support of my family and my wife. I am deeply indebted to my fiance, Lu Zhang. Throughout the years since we met, your love and support are beyond word. During these three years, we separate with each other in different country. Thank you for understanding me, believing me and encouraging me. This work is a successful result of our joint effort. Together we will have more stories of success in the rest of our life.

Last, but not least, I would like to thank Assister Prof. A. Takita, Dr. Azami and all my present and past LMM group colleagues for their participation in serve of my presentations, valuable suggestions, inspiring discussions with me and help in my life in Japan.

March 2013 Tao Jin

References

[1] Y. Fujii and H. Fujimoto, Measurements of frictional characteristics of a pneumatic linear bearing, *Measurement Science and Technology*, Vol.10, pp.362–366, 1999.

[2] Y. Fujii and H. Fujimoto, Proposal for an impulse response evaluation method for force transducers, *Measurement Science and Technology*, Vol.10, pp. N31–33, 1999.

[3] Y. Fujii, Measurement of force acting on a moving part of a pneumatic linear bearing, *Review of Scientific Instruments*, Vol.74, pp.3137–3142, 2003.

[4] Y. Fujii, Measurement of impulse response of force transducers, *Review of Scientific Instruments*, Vol.72, pp.3108–3111, 2001.

[5] Y. Fujii, Measurement of steep impulse response of a force transducer, *Measurement Science and Technology*, Vol 14, pp.65–69, 2003.

[6] Y. Fujii, Possible application of mass levitation to force measurement, *Metrologia*, Vol.38, pp.83–84, 2001.

[7] T. Bruns and M. Kobusch, Impulse force calibration: design and simulation of a new calibration device, *Proc. 17th IMEKO TC3 Conf.*, Istanbul, Turkey, pp.85-91, 2001.

[8] R. Kumme, Investigation of the comparison method for the dynamic calibration of force transducers, *Measurement*, Vol.23, pp.239–245, 1998.

[9] R. Kumme and M Dixon, The results of comparisons between two different dynamic force measurement systems, *Measurement*, Vol.10, pp.140–144, 1992.

[10] Y.K. Park, R. Kumme and D.I. Kang, Dynamic investigation of a three-component force-moment sensor, *Measurement Science and Technology*, Vol.13, pp.654–659, 2002.

[11] Y.K. Park, R. Kumme and D.I. Kang, Dynamic investigation of a binocular six-component force-moment sensor, *Measurement Science and Technology*, Vol.13, pp.1311–1318, 2002.

[12] Y. Fujii, A method for calibrating force transducers against oscillation force, *Measurement Science and Technology*, Vol.14, pp.1259–1264, 2003.

[13] Y. Fujii, Proposal for a step response evaluation method for force transducers, *Measurement Science and Technology*, Vol.14, pp.1741–1746, 2003.

[14] K.J. Xu and L. Jia, One-stage identification algorithm and two-step compensation method of Hammerstein model with application to wrist force sensor, *Review of Scientific Instruments*, Vol.73, pp.1949–1955, 2002.

[15] L. Zhang and R. Kumme. Investigation of a Homodyne and a Heterodyne Laser Interferometer for Dynamic Force Measurement, *Proc. SPIE 5503, Sixth International Conference on Vibration Measurements by Laser Techniques: Advances and Applications*, Vol. 5503, 2004.

[16] Y. Fujii, D. Isobe, S. Saito, H. Fujimoto, Y. Miki, A method for determining the impact force in crash testing, *Mechanical Systems and Signal Processing*, Vol.14, pp.959–965, 2000.

[17] Y. Fujii, Dynamic three-point bending tester using inertial mass and optical interferometer, *Optics and Lasers in Engineering*, Vol.38, pp.305–318, 2002

[18] Y. Fujii and T. Yamaguchi, A method for evaluating material viscoelasticity, *Review of Scientific Instruments*, Vol.75, pp.119–123, 2004.

[19] T. Suzuki, Y. Fujii and J.D.R. Valera, Optical method for strength test for general industrial products, *Mechanical Systems and Signal Processing* (to be submitted).

[20] Y. Fujii, Method of generating and measuring static small force using down-slope component of gravity, *Review of Scientific Instruments.*, Vol.78, pp.1935–1940, 2007.

[21] Y. Fujii and J. Valera Impact force measurement using an inertial mass and a digtizer, *Measurement Science and Technology.*, Vol.4, pp.863–868, 2006.

[22] Y. Fujii, K. Maru and J. Tao, Method for evaluating the electrical and mechanical characteristics of a voice coil actuator, *Precision Engineering*, Vol.4, pp.802–806, 2010.

[23] C. Schonenberger and S. F. Alvarado, A differential interferometer for force microscopy, *Review of Scientific Instruments.*, Vol.60, pp.3131–3134, 1989.

[24] B. Boashash, Estimating and interpreting the instantaneous frequency of a signal—part 1: Fundamentals, *Proceeding of the IEEE*, Vol.80, pp.520–538, 1992.

[25] D. Griffin and J. Lim, Signal estimation from modified short-time fourier transform, *IEEE Transactions on Acoustics, Speech, and Signal Processing*, Vol.32, pp.236–243, 1984.

[26] O. Besson and Galtier, Estimating particles velocity from laser measurments: maximun likelihood and Cramér-Rao bounds, *IEEE Transactions on Signal Processing.*, Vol.12, pp.3056–3068, 1996.

[27] B. Barkat and B. Boashash, Instantaneous frequency estimation of polynomial FM signals using the peak of the PWVD: statistical performance in the presence of additive Gaussian noise, *IEEE Transactions on Signal Processing.*, Vol.47, pp.2480–2490, 1999.

[28] B. Lehmann, H. Nobach and C. Tropea, Measurement of acceleration using the laser Doppler technique, *Measurement Science and Technology.*, Vol.13, pp.1367–1381, 2002.

[29] V. Friedman, A zero crossing algorithm for the estimation of the frequency of a signal sinusoid in white noise, *IEEE Transactions on Signal Processing.*, Vol.42, pp.1565–1569, 1994.

[30] F. Friedman, A zero crossing algorithm for estimation of the frequency of a single sinusoid in white noise, *IEEE Transactions on signal processing*, Vol.42, pp.1565–1569, 1994.

[31] Y. Fujii, and J. P. Hessling, Frequency estimation method from digitized waveform, *Experimental Techniques.*, Vol.33, pp.64–69, 2009.

[32] C. Mellet, J. C. Valiere and V. Valeau Use of frequency trackers in laser Doppler velocimetry for sound field measurement: comparative study of two estimators *Mechanical Systems and Signal Processing*, Vol.17, pp.329–344, 2003.

[33] V. Valeau, J. C. Valiere and C. Mellet, Instantaneous frequency tracking of a sinusoidally frequency-modulated signal with low modulation index: application to laser measurements in acoustics, *Signal Processing*, Vol.84, pp.1147–1165, 2004.

[34] B. Boashash Estimating and interpreting the instantaneous frequency of a signal—part 2: Algorithms and Application, *Proceeding of the IEEE*, Vol.80, pp.540–568, 1992.

[35] C. M. Caves Quantum-mechanical noise in an interferometer, *Physical Review D.*, Vol.23, pp.1693-1708, 1981.

[36] R. Kowalski, S. Root, S. D. Gensemer and P. L. Gould, A frequency-modulated injection-locked diode laser for two-frequency generation, *Review of Scientific Instruments.*, Vol.72, pp.2532–2534, 2001.

[37] L. M. Barker and R. E. Hollenbach, Laser interferometer for measuring high velocities of any reflecting surface, *Journal of Applied Physics*, Vol.43, pp.4669–4675, 1992.

[38] Y. Fujii, An optical method for evaluating frictional characteristics of linear bearing, *Optics and Lasers in Engineering*, Vol.42, pp.493-501, 2004.

[39] E. Durak, C. Kurbanoğlu, A. Bıyıklıoğlu and H. Kaleli, Measurement of friction force and effects of oil fortifier in engine journal bearings under dynamic loading conditions, *Tribology International*, Vol. 36, pp.599–607, 2003

[40] B.S. Ünlü, and E. Atik, Determination of friction coefficient in journal bearings, *Materials & Design*, Vol. 28, pp.973-977, 2007.

[41] Z. Yao, Q. Zhang, Y. Tao and X. Zhang, A new approach to measure the friction coefficient of micro journal bearings, *Tribology International*, Vol. 33, pp.485-489, 2000.

[42] K. Budinski, An inclined plane test for the breakaway coefficient of rolling friction of rolling element bearings, *Wear*, Vol. 259, pp.1443-1447, 2005.

[43] Y. Fujii, Measurement of force acting on a moving part of a pneumatic linear bearing, *Review of Scientific Instruments*, Vol. 74, pp.3137-3141, 2003.

[44] Y. Fujii, Frictional characteristics of an aerostatic linear bearing, *Tribology International*, Vol. 39, pp.888-896, 2006.

[45] Y. Fujii, An optical method for evaluating frictional characteristics of linear bearings, *Optics and Lasers in Engineering*, Vol. 42, pp.493-501, 2004.

[46] T. Baumeister, and L. S. Marks, Standard handbook for mechanical engineers, Seventh Edition, Section 3, McGraw-Hill, New York, 1967.

[47] Y. Fujii, and J. Valera, Impact force measurement using an inertial mass and a digitizer, *Measurement Science and Technology*, Vol. 17, pp.863-868, 2006.

[48] Y. Fujii, Impact response measurement of an accelerometer, *Mechanical Systems and Signal Processing*, Vol. 21, pp.2072-2079, 2007.

[49] Y. T. Liu, R. F. Fung and C. C. Wang, Precision position control using combined piezo-VCM actuators, *Precision Engineering*, Vol.29, pp. 411–422, 2005.

[50] H. W. Park, H. S. Yang, Y. P. Park and S. H. Kim, Position and vibration control of a flexible robot manipulator using hybrid controller, *Robotics and Autonomous Systems*, Vol.28, pp.31–41, 1999.

[51] Oriol Gomis-Bellmunt, Samuel Galceran-Arellano, Antoni Sudri´a-Andreu, Daniel Montesinos-Miracle and L. Flavio Campanile, Linear electromagnetic actuator modeling for optimization of mechatronic and adaptronic systems, *Mechatronics*, Vol.17, pp.153–163, 2007.

[52] R. Gollee, Th. Roschke and G. Gerlach, A finite element method based dynamic analysis of a long-stroke linear actuator, *Journal of Magnetism and Magnetic Materials*, Vol.196–197, pp.943-945, 1999.

[53] Y. Fujii, Measurement of steep impulse response of a force transducer, *Meas. Sci. Technol.*, Vol. 14, No.1 pp. 65-69, 2003.

[54] Y. Fujii, Measurement of the electrical and mechanical responses of a force transducer against impact forces, *Review of Scientific Instruments*, Vol.77, pp. 085108-1-5, 2006.

[55] Y. Fujii, Frictional characteristics of an aerostatic linear bearing, Tribology International, Vol.39, pp.888–896, 2006.

[56] Y. Fujii, Microforce materials tester, *Review of Scientific Instruments*, Vol.76, No.6, 065111-1-7, 2005.

[57] Y. Fujii, Method of evaluating the dynamic response of materials to forced oscillation, *Measurement Science and Technology*, Vol.17, pp. 1935–1940, 2006.

[58] Y. Fujii, Impact response measurement of an accelerometer, *Mechanical Systems and Signal Processing*, Vol.21, pp.2072–2079, 2007.

[59] J. Juuti, K. Kordäs, R. Lonnakko, V.P. Moilanen and S. Leppävuori, Mechanically amplified large displacement piezoelectric actuators, *Sensors and Actuators A: Physical.*, Vol.120, pp. 225–231, 2005.

[60] Y.T. Liu, R.T . Fung, C.C. Wang, Precision position control using combined piezo-VCM actuators, *Precision Engineering.*, Vol.29, pp.411–422, 2005.

[61] V. G. M. Annamas and C. Soh, An electromechanical impedance model of a piezoceramic transducer-structure in the presence of thick adhesive bonding, *Smart Materials and Structures.*, Vol.16, pp.673–686, 2007

[62] C. Liang, F. P. Sun, C. A. Rogers, Dynamic analysis of active material systems, *Journal of Intelligent Material Systems and Structures.*, Vol.8, pp.323–334, 1997.

[63] V. Giurgiutiu, C. A. Rogers, Power and energy characteristics of soild-state induced-strain actuators for static and dynamic application, *Journal of Intelligent Material Systems and Structures*, Vol.8, pp.738–750, 1997.

[64] R. Pomirleanu, V. Giurgiutiu, Full-stroke static and dynamic analysis of high-power piezoelectric actuators, *Journal of Intelligent Material Systems and Structures*, Vol.13, pp.275–289, 2002.

[65] Mechanical Considerations for Dynamic Operation of PZTs, *Available online: http://www.physikinstrumente.com/tutorial*, 23 August, 2012.

[66] M. Fouaidy, G. Martinet, N. Hammoudi, F. Chatelet, S. Blivet, A. Olivier, H. Saugnac, Full Characterization at Low Temperature of Piezoelectric Actuators Used for SRF Cavities Active Tuning. In *Proceedings of the Particle Accelerator Conference 2005*, Knoxville, USA, 16–20 May pp.728–730, 2005 .

[67] S. B. Choi, S. B. Hong and Y. M. Han, Dynamic characteristics of intertial actuator featuring piezoelectric materials: Experimental verification, *The Journal of Sound and Vibration.*, Vol. 302, pp.1048–1056, 2007.

[68] J. J. Tzen, S. L. Jeng, and W. H. Chieng, Modeling of piezoelectric actuator for comensation and controller design, *Precision Engineering.*, Vol.27, pp.70–86, 2003

[69] H. Moilanen and S. Leppävuori, Laser interferometric measurement of displacement-field characteristics of piezoelectric actuators and actuator materials, *Sensors and Actuators A: Physical.*, Vol.92, pp. 326–334, 2001

[70] D. H. Zhang, Y. G. Yu, H. Y. Ye, Measuring the dynamic performance of PZT using self-mixing interference vibrometer, *Journal of Optoelectronics Laser*, Vol.16, pp.714–717, 2005, in Chinese.

[71] Y. Fujii, Microforce materials tester based on the levitation mass method, *Measurement Science and Technology.*, Vol.18, pp.1678–1682, 2007.

[72] Y. Fujii, K. Maru, and T. Jin, Method for evaluating the electrical and mechanical characteristics of a voice coil actuator, *Precision Engineering.*, Vol.34, pp.802–806, 2010.

[73] Y.T. Ma, L.Huang, and W. W. Shao, New open loop control improves linearity of piezoelectric actuators, *Advanced Materials Research.*, Vol.34, pp.520–524, 2010.

[74] T. Miysako, B.N. Trinh, M. Onoue, T. Kaneda, P. T. Tue, E. Tokumits, and T. Shimoda, Ferroelectric-gate thin-film transistor fabricated by total solution deposition process, *Japanese Journal of Applied Physics.*, Vol.50, doi:10.1143/JJAP.50.04DD09, 2011.

[75] J.T . Royston, Modeling and measurement of nonlinear dynamic behavior in piezoelectric ceramics with application to 1-3 composites, *Journal of the Acoustical Society of America.*, Vol.104, pp.2814–2827, 1998.

[76] M. Goldfard, and N. Celanovic, Modeling piezoelectric stack actuators for control of micromanipulation. *IEEE Control System.*, Vol.17, pp.69–79, 1997.

[77] Y. Fujii, T. Jin, S. Mitatha, P. P. Yupapin, W. M. Hou, T. Yamaguchi, Review of the Levitation Mass Method a Precision Mechanical Measurement Method, *Procedia Engineering*, Vol.8, pp.504–510, 2011.

[78] Y. Fujii, Toward establishing dynamic calibration method for force transducers, *IEEE Transactions on Instrument and Measurement*, Vol.58, pp.2358–2364, 2009.

[79] Y. Fujii and T. Yamaguchi, Method for evaluating material viscoelasticity, *Review of Scientific Instruments.*, Vol.75, pp.119–123, 2004.

[80] B. Gu, D. Shu, Y. Fujii and B. Shi, Dynamic force measurement of a head arm assembly of a hard disk drive by numerical analysis and experiments, *IEEE Transactions on Magnetics.*, Vol. 45, pp.5034–5037, 2009.

[81] R. W. Peterson, G. M. Robinson, R. A. Carlsen, C. C. Englund, P. J. Moran and W. M. Wirth, Interferometric measurements of the surface profile of moving samples, *Applied Optics.*, Vol.23, pp.1464–1466, 1984.

[82] S. L. Zhang, M. X. Wu and G. F. Jin, Birefringent tuning double frequency He-Ne laser, *Applied Optics.*, Vol.29, pp.1265–1267, 1990.

[83] G. Xiao, X. Long and B. Zhang, Precise force measurement method by a Y-shaped cavity dual-frequency laser, *Chinese Optics Letters*, Vol. 9, pp. 101201, 2011.

[84] A. Takita, H. Ebara and Y. Fujii, Dual beat-frequencies laser Doppler interferometer, *Review of Scientific Instruments.*, Vol.82, pp.123111, 2011.

[85] L. Zhang and R. Kumme. Investigation of a Homodyne and a Heterodyne Laser Interferometer for Dynamic Force Measurement, *Proc. SPIE 5503, Sixth International Conference on Vibration Measurements by Laser Techniques: Advances and Applications*, Vol. 5503, 2004.

Publication list

Publications related to the thesis

1. T. Jin, A. Takita, M. Djamal, W. Hou, H. Jia and Y. Fujii, A method for evaluating the electro-mechanical characteristics of piezo-electric actuators during motion. *Sensors*, Vol.12, No. 9, pp.11559–11570, 2012.

2. Y. Fujii, K. Maru, T. Jin, P. P. Yupapin and M. Somsak, A Method for Evaluationg Dynamical Friction in Linear Ball Bearings, *Sensors*. Vol.10, No.11, pp.10069–10080, 2010.

3. Y. Fujii, K. Maru and T. Jin, Method for evaluating the electrical and mechanical characteristics of a voice coil actuator. *Precision Engineering*. Vol.34, No.4, pp: 802–80, 2010.

Other publications

1. Y. Fujii, T. Jin, S. Mitatha, P. P. Yupapin, W.M. Hou, T. Yamaguchi, Review of the Levitation Mass Method a Precision Mechanical Measurement Method, *Procedia Engineering*, Vol.8, pp.504–510, 2011.

2. Y. Fujii, K. Maru, K. Shimada, T. Jin and W. Thornton, Space Balance and Space Scale: Mass Measurement Devices MMDs, *Applied Mechanics and Materials*, Vol.36, pp.31-40, 2010.

3. Y. Fujii, K. Maru, T. Jin and T. Yamaguchi, Precision Force Measurement Using the Levitation Mass Method (LMM), *Applied Mechanics and Materials*, Vol.36, pp.41–51, 2010.

4. T. Jin, H. Z. Jia, W. M. Hou, R. Yamamoto, N. Nagai, Y. Fujii, K. Maru, N. Ohta and K. Shimada, Evaluating 3D position and velocity of subject in parabolic flight experiment by use of the binocular stereo vision measurement. *Chinese Optics Letter*, Vol.8, No.6, pp.601-605, 2010.

5. T. Jin, H. Z. Jia, W. M. Hou, R. Yamamoto, N. Nagai and Y. Fujii, Study on Extraction Method of The Circle Outline and Its Center In a Moving Dummy Mass, *Electronics world*. vol.116 pp.22-25, 2010

6. T. Jin, H. Z. Jia, W. M. Hou, R. Yamamoto, N. Nagai, Y. Fujii, K. Maru, N. Ohta and K. Shimada, Motion Pose Estimated Based on the Binocular Stereo Camera, *Applied Mechanics and Materials*, Vol.36 pp.494-496, 2010

7. T. Jin, H. Z. Jia, R. Yamamoto, N. Nagai, Y. Fujii, K. Maru, K. Shimada, The extraction method of moving circle and circle center research, *Laser Journal*, Vol.4 pp.24-26, 2010

8. T. Jin, H. Hoshino, Y. Fujii, H. Z. Jia, K. Maru and W. M. Hou, Color estimation base on a giving color estimation PC-based system, *Procedia-Social and Behavioral Sciences 2(1)*. Vol. 2, pp.120-124, 2009

Conference

1. T. Jin, A. Takita, M. Djamal, W. Hou, H. Jia and Y. Fujii, Dynamic analysis of the electromechanical characteristic of piezoelectric actuators using an interference method, *4th International Conference on Advanced Micro-Device Engineering*, 2011